

Efficiency of Nonlinear Particle Acceleration at Cosmic Structure Shocks

Hyesung Kang

Department of Earth Sciences, Pusan National University, Pusan 609-735, Korea

kang@uju.es.pusan.ac.kr

and

T.W. Jones

Department of Astronomy, University of Minnesota, Minneapolis, MN 55455

twj@msi.umn.edu

ABSTRACT

We have calculated the evolution of cosmic ray (CR) modified astrophysical shocks for a wide range of shock Mach numbers and shock speeds through numerical simulations of diffusive shock acceleration (DSA) in 1D quasi-parallel plane shocks. The simulations include thermal leakage injection of seed CRs, as well as pre-existing, upstream CR populations. Bohm-like diffusion is assumed. We model shocks similar to those expected around cosmic structure pancakes as well as other accretion shocks driven by flows with upstream gas temperatures in the range $T_0 = 10^4 - 10^{7.6}$ K and shock Mach numbers spanning $M_s = 2.4 - 133$. We show that CR modified shocks evolve to time-asymptotic states by the time injected particles are accelerated to moderately relativistic energies ($p/mc \gtrsim 1$), and that two shocks with the same Mach number, but with different shock speeds, evolve qualitatively similarly when the results are presented in terms of a characteristic diffusion length and diffusion time. We determine and compare the “efficiencies” of CR acceleration in our simulated shocks by calculating the ratio of the total CR energy generated at the shock to the total kinetic energy that would pass through the shock over time in its initial frame of reference. For these models the time asymptotic value for this efficiency ratio is controlled mainly by shock Mach number, as expected from the aforementioned similarity in CR

¹Submitted to the Astrophysical Journal

shocks. In the presence of a pre-existing CR population, shock evolution proceeds similarly to that for higher thermal injection rates compared to thermal leakage CR sources alone. This added contribution has little or no impact on the post-shock or CR properties of the high Mach number shocks simulated. The modeled high Mach number shocks all evolve towards efficiencies $\sim 50\%$, regardless of the upstream CR pressure. On the other hand, the upstream CR pressure increases the overall CR energy in moderate strength shocks ($M_s \sim$ a few), since it is a significant fraction of the shock ram pressure. These shocks have been shown to dominate dissipation during cosmic structure formation, so such enhanced efficiency could significantly increase their potential importance as sources of cosmic rays.

Subject headings: acceleration of particles–cosmic rays– hydrodynamics– methods:numerical

1. Introduction

Collisionless shocks form ubiquitously in tenuous cosmic plasmas via collective, electromagnetic viscosities. The formation process of such shocks inevitably produces suprathermal particles in addition to thermal particles with Maxwellian velocity distributions (Blandford and Eichler 1987; Jones and Ellison 1991; Draine and McKee 1993). These nonthermal particles can be further accelerated to very high energies through the interactions with resonantly scattering Alfvén waves in the converging flows across a shock, *i.e.*, by diffusive shock acceleration (DSA) (Drury 1983; Blandford and Eichler 1987; Malkov and Drury 2001). Detailed nonlinear treatments of DSA predict that a small fraction of incoming thermal particles can be injected into the CR population, and that a significant fraction of the shock kinetic energy can be transferred to CRs (*e.g.*, Ellison, Baring & Jones 1995; Kang, Jones, and Gieseler 2002).

Simulations of DSA in spherical supernova remnants (SNRs) indicate that CRs can absorb up to 50% of the initial blast energies (*e.g.*, Berezhko and Völk 1997, 2000). Support for rapid and efficient DSA in that setting has been provided by recent X-ray observations of young SNRs such as SN1006 and Cas A that indicate the presence of short-lived, TeV electrons emitting nonthermal synchrotron emission immediately inside the outer SNR shock (Koyama et al. 1995; Allen et al. 1997; Bamba et al. 2003). On a galactic scale it is well known that the CR energy density is comparable to the gas thermal energy density in the interstellar medium and plays important dynamical roles in the evolution of our Galaxy. Although the Galactic CRs are commonly believed to be accelerated mostly at SNR shocks,

CR acceleration is probably important in all shock-heated astrophysical plasmas.

CR populations are also indicated by extended, diffuse nonthermal emissions in some galaxy clusters (*e.g.*, Miniati et al. 2001, and references therein). One likely contribution to that CR population is large scale shocks associated with the formation of the clusters. According to hydrodynamic simulations of large scale structure formation in the universe, nonlinear structures such as pancakes, filaments, and knots are surrounded by “external” accretion shocks and contain complex webs of “internal” flow shocks including, but not limited to, accretion shocks around individual clusters and merger shocks inside clusters (Miniati et al. 2000). Recently, Ryu et al. (2003) studied the characteristics of such cosmic shocks and showed that they have a wide range of physical parameters with shock speeds, u_s , up to $\sim 3000 \text{ km s}^{-1}$, preshock temperatures of $10^4 < T_0 < 10^8 \text{ K}$, and Mach numbers up to a few 100. They showed that in the present universe the mass inside nonlinear structures has been shocked approximately twice on average over cosmic time, and that shocks with $2 \lesssim M \lesssim 4$ have contributed $\sim 1/2$ of the total energy dissipated at the shocks. Utilizing nonlinear DSA model calculations of Kang, Jones, and Gieseler (2002), Ryu *et al.* estimated that the ratio of CR energy to gas thermal energy resulting from dissipation at cosmological shocks is $\sim 1/2$. Hence, the CR energy density could be dynamically important in the intracluster medium, just as in the interstellar medium of our Galaxy and might have had some dynamical influences on large scale structure formation.

The above “cosmic structure shocks” are an inevitable consequence of gravitational collapse, and are central to virialization of diffuse baryonic matter. The DSA process behind our present discussion depends, of course, on the existence of a magnetic field in the shock vicinity to mediate Alfvénic turbulence that scatters the CRs. The effectiveness of the scattering at a particular particle momentum, $p = \gamma v m$, can be expressed in terms of the DSA diffusion time, $t_d(p) = \kappa(p)/u_s^2$, where $\kappa = (1/3)r_g v (B/\delta B)^2$ is the spatial diffusion coefficient, $r_g = pc/(eB)$ is the particle gyroradius, B is the magnetic field, and δB characterizes the magnitude of resonant wave magnetic fields. Particles will generally be accelerated from low energies to $E \sim pc$ on timescales a few times $t_d(p)$ (see equation 2). Efficient transfer of kinetic energy to CRs typically becomes apparent in DSA simulations by the time transrelativistic CRs are accelerated, establishing the relevant time scale for the introduction of nonlinear feedback into the shock dynamics.

Evidence is strong that magnetic fields exist in clusters at levels exceeding at least a few $\times 10^{-7} \text{ Gauss}$ (*e.g.*, Kronberg 2001). Fields of that strength lead, with Bohm diffusion ($\delta B = B$), to diffusion times for transrelativistic CRs, $t_d = (1/3)pcv/(eBu_s^2)$ of the order of a few years for $p \sim mc$ in fast cosmic shocks with speeds $\sim 10^3 \text{ km s}^{-1}$.

Direct evidence for microGauss-level magnetic fields where most cosmological shocks

form, that is, outside individual clusters, is currently quite limited. However, there are good reasons to expect fields adequate for efficient DSA in most cosmic shocks. For example, even in the absence of any primordial seed field, magnetic fields are likely to be spontaneously generated at “external cosmic shocks” by some combination of the Biermann battery (Kulsrud et al. 1997; Ryu, Kang & Biermann 1998) and the Weibel instability (Schlickeiser & Shukla 2003). Whether such seed fields are initially strong enough to reduce diffusion times to cosmologically interesting values or not, quasi-linear plasma theory and simulations show that the streaming motion of suprathermal particles can induce resonant Alfvén wave generation and strong field amplification upstream of collisionless shocks (*e.g.*, Bell 1978; Quest 1988; Lucek and Bell 2000; Bell and Lucek 2001). Bell and Lucek (2001) have argued that magnetic fields can ultimately be amplified to produce magnetic pressures that are a substantial fraction of the ram pressure through the shock, $\rho_0 u_s^2$. That limit would correspond to field strengths $\sim 4 \times 10^{-7} h(1 + \delta)^{1/2} u_{s,3}(1 + z)^{3/2}$ Gauss, where h is the Hubble parameter in units of 100 km/sec/Mpc, $\delta = \delta\rho/\rho$ is the local overdensity ratio, z is the redshift of the epoch, and $u_{s,3}$ is the shock speed in units of 10^3 km s $^{-1}$. A baryon density fraction, $\Omega_b = 0.04$, is assumed. Even magnetic fields only one percent of this value would be sufficient to accelerate CRs to relativistic energies, and, hence establish nonlinear CR feedback on timescales of thousands of years in the shocks of interest.

Once shocks develop nonlinear properties in response to CR feedback, there are several important characteristics that distinguish them from more familiar gasdynamic shocks: 1) CR shocks continue to evolve over relatively long times and broaden as they do so. While full thermalization takes place instantaneously at a simple, discontinuous jump in an “ideal” gasdynamic shock, CR acceleration and the corresponding modifications to the underlying flow depend on suprathermal particles passing back and forth diffusively across the shock structure. These processes develop, therefore, on the diffusion time scale, t_d , and diffusion length scale, $x_d = t_d u_s$, as alluded to earlier. Generally, these scales are expected to be increasing functions of particle momentum, so CR acceleration and shock evolution rates slow over time. For very high energy particles DSA time and length scales often approach the age and the radius of curvature of astrophysical shocks. 2) CR diffusion upstream of the shock discontinuity leads to strong pressure gradients in a shock precursor, enhancing the total compression through the shock transition over that in the “viscous” subshock. The total compression through a high-Mach-number CR shock can greatly exceed the canonical value $r = (\gamma_g + 1)/(\gamma_g - 1)$ for strong gasdynamical shocks (*e.g.*, Berezhko and Ellison 1999; Malkov, Diamond & Völk 2000) (where γ_g is the gas adiabatic index). 3) Both the effective compressibility of the combined thermal-CR plasmas and the mean CR diffusion coefficient increase over time as relativistic CRs absorb more energy and as escaping CRs remove energy from the shock structure. Details of these properties depend on the CR momentum

distribution. Thus, downstream states of the CR modified shock cannot be found from simple “shock jump conditions”, but rather have to be integrated time-dependently from given initial states or, for steady solutions, found in terms of some predefined limits to the CR spectrum (*e.g.*, an upper momentum cutoff). 4) Energy transfer to the CRs rather than to the thermalized gas in the shock transition reduces the downstream thermal energy of a CR modified shock compared to a gasdynamic shock with the same shock speed and Mach number. The Mach number of the gas subshock is also reduced. Even in a shock with a very large total Mach number, the subshock Mach number and compression ratio are typically ~ 3 (*e.g.*, Malkov 1998; Berezhko and Ellison 1999; Kang, Jones, and Gieseler 2002).

In order to study these processes closely we recently developed a numerical scheme that self-consistently incorporates a thermal leakage CR injection model based on the analytic, nonlinear calculations of Malkov (1998) (Gieseler et al. 2000) and implemented it into a combined Adaptive Mesh Refinement (AMR) gas dynamics and CR diffusion-convection code (Kang, Jones, and Gieseler 2002). As described in the following section, there is only one rather well constrained parameter needed to express this injection model; namely, the strength of nonlinear MHD waves immediately downstream of the plasma subshock with respect to the upstream longitudinal magnetic field strength.

Previously, we applied our new code to a preliminary investigation of cosmic shocks emerging in large scale structure formation of the universe (Kang and Jones 2002; Kang 2003). Utilizing the Bohm diffusion model in 1D quasi-parallel, plane-parallel shocks we showed that the resulting CR modified shocks evolve roughly “self-similarly” if the shock structure is expressed in terms of diffusion time and length scales, and that the time asymptotic states depend mainly on the shock Mach number, with only a weak dependence on the parameter needed in the injection model. We found for strong shocks that about 10^{-3} of incoming thermal particles are injected into the CR population with our thermal leakage injection model over the long term, and up to $\sim 1/2$ of the shock kinetic energy flux measured in the initial shock frame is transferred to CRs. In the present contribution we confirm and extend our previous studies by including simulations of shock models with a broader range of physical parameters suitable for application to cosmic structure formation shocks, and also by including the influence of a pre-existing, upstream CR population, since many of the shocks of interest will probably form in previously shocked plasma. Our numerical simulations here are limited to quasi-parallel shocks in which the mean magnetic field lines are parallel to the direction of shock propagation. In quasi-planar shocks this is not a strong limitation so long as the obliquity of the magnetic field is small enough to keep its intersection subluminal and so long as the magnetic field is too weak to be dynamically important (*e.g.*, Jokipii 1982; Drury 1983). In addition, since streaming motions inside cosmic sheets and filaments appear to stretch the field lines (*e.g.*, Ryu, Kang & Biermann 1998), many

structure formation “internal” shocks are likely to be quasi-parallel. The principle concern may be the influence of obliquity on the injection of low energy CRs at the shocks, as we discuss below.

In the following section we briefly outline our numerical methods in the CR/AMR hydrodynamics code. The simulation results are presented and discussed in §3, followed by a summary in §4.

2. Numerical Calculations

2.1. The CRASH code

Our conservative, Eulerian CR/AMR hydrodynamics code, CRASH (Cosmic-Ray Amr SHock), solves the gasdynamic equations with CR pressure terms added for one dimensional plane-parallel geometry, along with the diffusion-convection equation for the CR momentum distribution function, $g(p) = f(p)p^4$. The full CR shock transition includes a very wide range of length scales associated with the particle diffusion lengths that must be resolved to follow the shock evolution properly. To include CRs injected by thermal leakage, these scales must extend down close to the subshock thickness. In order to handle this dynamic range efficiently, an adaptive mesh refinement (AMR) technique is applied to regions around gasdynamic shocks, which are tracked as discontinuous jumps by a front-tracking method (Kang et al. 2001). An additional equation for the “Modified Entropy”, $S = P_g/\rho^{\gamma_g-1}$, is solved to follow accurately the adiabatic changes outside of shocks, particularly in the precursor region of strong shocks (Kang, Jones, and Gieseler 2002). Readers are referred to these previous papers for further numerical details.

2.2. The Bohm Diffusion Model

DSA, along with the time and length scales for CR acceleration, and subsequent shock modification, depend on the spatial diffusion coefficient for the CRs. The diffusion coefficient can be expressed in terms of a mean scattering length, λ , as $\kappa(x, p) = \frac{1}{3}\lambda v$, where v is the particle velocity. As noted earlier, for Alfvén wave scattering one can write $\lambda \approx r_g(B/\delta B)^2$ (*e.g.*, Skilling 1975). The Bohm diffusion model, representing a saturated wave spectrum ($\delta B \sim B$) and the minimum diffusion coefficient, gives $\kappa_B = (1/3)r_g v$. If we assume “Bohm-like” diffusion with $\lambda = \zeta \times r_g$ with $\zeta \geq 1$, the diffusion coefficient can be expressed as

$$\kappa(\rho, p) = \kappa_n \left(\frac{\rho_0}{\rho} \right) \frac{p^2}{(p^2 + 1)^{1/2}}, \quad (1)$$

where hereafter momentum, p , is expressed in units of mc and $\kappa_n = \zeta \times (1/3)mc^2/(eB)$, represents the diffusion coefficient far upstream of the shock for CRs with $p \approx 1.3$. The assumed density dependence for κ accounts for compression of the perpendicular component of the wave magnetic field and also inhibits the acoustic instability in the precursor of highly modified CR shocks (Drury and Falle 1986; Kang, Jones and Ryu 1992). Also, hereafter, we use the subscripts '0', '1', and '2' to denote conditions far upstream of the shock, immediately upstream of the gas subshock and immediately downstream of the subshock, respectively. Thus, ρ_0 represents the far-upstream gas density.

The so-called DSA diffusion time, $t_d = \kappa/u_s^2$, defined in the introduction represents the time scale for hydrodynamical advection across the CR diffusion length, x_d , which, in turn represents the length on which CR diffusion upstream is balanced by advection towards the subshock. Conveniently, t_d also provides a natural time unit to measure the acceleration time for individual CRs. The residence time for individual particles on each side of the shock is proportional to x_d/v , while the CR fractional momentum gain per shock crossing pair is proportional to $\Delta u/v$. The resulting acceleration time scale for a particle to reach momentum p (*e.g.*, Drury 1983) is defined as

$$\tau_{acc}(p) = \frac{3}{u_1 - u_2} \left(\frac{\kappa_1}{u_1} + \frac{\kappa_2}{u_2} \right) \approx \frac{8M_s^2}{M_s^2 - 1} t_d(p) . \quad (2)$$

The approximate, Mach-number-based expression in equation (2) is based on the compression through a gasdynamic shock for $\gamma_g = 5/3$ and sets $u_s = u_1$. Once again, $t_d(p) = \kappa(p)/u_s^2$. Thus, the CR acceleration time depends on both the speed and the Mach number (actually compression) of the shock in addition to the diffusion coefficient. In the limit of strong shocks ($M_s \gg 1$), however, it becomes independent of the shock Mach number, and is about an order of magnitude greater than the nominal diffusion time, *i.e.*, $\tau_{acc} \approx 8t_d$. We note, however, that in CR modified shocks the compression factor across the total shock structure can be greater than that of strong gasdynamic shocks, and that higher energy CRs with greater diffusion length see a greater compression ratio. Consequently, the mean acceleration timescale at a fixed CR energy is somewhat smaller than that given in equation (2).

2.3. The Thermal Leakage Injection Model

In the “thermal leakage” model for CR injection at shocks, most of the downstream thermal protons are locally confined by nonlinear MHD waves and only particles well into the tail of the postshock Maxwellian distribution can leak upstream across the subshock (*e.g.*, Ellison and Eichler 1985; Malkov 1998; Malkov and Drury 2001). In particular, “leak-

ing” particles not only must have velocities large enough to swim against the downstream flow in order to return across the shock, they must avoid being scattered by the MHD waves that mediate the plasma subshock. The latter effect further strongly filters particles against leaking. Thus, the ratio of the breadth of the postshock thermal velocity distribution to the downstream flow velocity in the subshock rest-frame is central to the injection problem. Malkov and Völk (1998) and (Malkov 1998) developed a nonlinear analytic model to incorporate these features, and we have adapted that model to our simulations. In order to model this injection process numerically Gieseler et al. (2000) constructed a “transparency function”, $\tau_{\text{esc}}(\epsilon, v)$ that expresses the probability of supra-thermal particles at a given velocity, v , leaking upstream through the postshock MHD waves. One free parameter, defined by Malkov and Völk (1998), controls this function; namely, $\epsilon = B_0/B_\perp$, which is the ratio of the amplitude of the postshock MHD wave turbulence B_\perp to the general magnetic field aligned with the shock normal, B_0 . As noted by Malkov and Völk (1998) this parameter is rather well constrained, since $0.3 \lesssim \epsilon \lesssim 0.4$ is indicated for strong parallel shocks. However, such large values of ϵ lead to very efficient initial injection and most of the shock energy is quickly transferred to the CR component for strong shocks of $M_s \gtrsim 30$ (Kang and Jones 2002), causing a numerical problem at the very early stage of simulations. Consequently, we reduced the shock transparency by setting $\epsilon = 0.2$ in this study. Kang (2003) showed that time asymptotic states of the CR shocks depend only weakly on the values of ϵ in this range. On the other hand, smaller ϵ values may also be more in tune with behaviors in moderately oblique shocks, since finite magnetic field obliquity also reduces shock transparency and the rate of thermal injection (*e.g.*, Ellison, Baring & Jones 1995; Völk, Berezhko & Ksenofontov 2003). We note that Völk, Berezhko & Ksenofontov (2003) estimate that the injection rate for angles $\gtrsim 35^\circ$ falls below the critical injection rate for efficient shock modification, $\xi \sim 6 \times 10^{-5}$ (as defined in equation 5), and CR acceleration becomes very inefficient.

2.4. Normalization of Physical Variables

The ideal gasdynamic equations in 1D planar geometry do not contain any intrinsic time and length scales, but in CR modified shocks the CR acceleration and the precursor growth can be characterized by the diffusion scales, $t_d(p)$ and $x_d(p)$. $\kappa_n = \kappa(p \approx 1.3)$ provides a useful canonical value, since nonlinear feedback from CRs to the underlying flow becomes significant typically by the time transrelativistic CRs are accelerated. Consequently, we normalize our shock evolution times and structure scales by $t_n = \kappa_n/u_n^2$, and $x_n = \kappa_n/u_n$, respectively, where u_n is a characteristic flow speed. One expects intrinsic similarities in the dynamic evolution and structure of two CR shock models with the same Mach number, but

with different shock speeds, *so long as the results are expressed in terms of t_n and x_n* . This approach removes the need for any particular choice in κ_n , but we note for convenience that $\kappa_n = 3.1 \times 10^{23} \zeta / B_{-7} \text{ cm s}^2$, where $B = B_{-7} \times 10^{-7} \text{ Gauss}$. Then for example, a characteristic diffusion time, $t_n = \kappa_n / u_n^2 = 3.1 \times 10^7 \zeta / (B_{-7} u_{n,3}^2) \text{ sec}$, and $x_n = 3.1 \times 10^{15} \zeta / (B_{-7} u_{n,3}) \text{ cm}$, where $u_n = u_{n,3} \times 10^3 \text{ km/sec}$.

In the simulations described below we express pressures and energy densities in units $P_n = \rho_n u_n^2$, where ρ_n will be an appropriate fiducial gas density. Again, for reference, we can express these quantities in practical units in terms of the preshock cosmic overdensity ratio, δ , as $\rho_n \approx 7.5 \times 10^{-31} (1 + \delta) h^2 (1 + z)^3 \text{ g cm}^{-3}$ and $P_n \approx 7.5 \times 10^{-15} h^2 (1 + \delta) (1 + z)^3 u_{n,3}^2 \text{ dyne cm}^{-2}$, with the same cosmological choices mentioned in the introduction.

When the shock speeds are less than a percent or so of the speed of light, freshly injected CRs are essentially nonrelativistic ($p_{\text{inj}} \propto \sqrt{T_2} \propto (u_s/c)$), so both the diffusion coefficient and CR partial pressure take power law forms; thus, allowing self-similar behaviors in modified shock evolution. On the other hand, once the shock speed exceeds a percent or so of the speed of light, the full expression for the particle speed, $v = p/\sqrt{p^2 + 1}$, must be applied, so neither the diffusion coefficient nor the CR partial pressure permit self-similar scalings. Consequently, the physical shock speed does influence the evolution of the fastest shocks we simulated in this study.

2.5. Simulation Set Up and Model Parameters

We model shocks that form in an accretion flow entering through the right boundary in a 1D simulation box, $[0, x_{\text{max}}]$. The inflow has constant density, speed, and pressure. This flow reflects off the left boundary, or piston, to initiate the shock, which evolves in response to CRs accelerated via DSA as it propagates to the right. With the normalization constants described above, $\tilde{\rho}_0 = 1$, $\tilde{u}_0 = -1$, and $\tilde{P}_{g,0} = (1/\gamma_g) M_0^{-2}$ in code units, where M_0 is the accretion flow Mach number. The gas adiabatic index, $\gamma_g = 5/3$. The shock normalization constants are set by two parameters, M_0 and $c_{s,0}$, through

$$u_n = |u_0| = c_{s,0} M_0, \quad (3)$$

where $c_{s,0} = 15 \text{ km s}^{-1} (T_0/10^4)^{1/2}$ is the upstream sound speed of the accretion flow. We assume the preshock gas is fully ionized with a mean molecular weight, 0.61. We do not include complexities due to interactions between neutral and ionized gas in our numerical treatment. We also ignore added energy transport processes such as radiative cooling, the diffuse radiation emitted by the shock-heated gas and thermal conduction. However, they should be included in future studies for more realistic model calculations.

For a gasdynamic shock with compression ratio, r , the speed of the shock reflected from the piston is $u_s = u_n/(r-1)$ in the piston (*i.e.*, simulation) frame and $u'_s = u_n r/(r-1)$ in the upstream flow frame. From this relation, the *initial* shock speed with respect to the upstream flow spans the range $u'_{s,0} = (4/3 - 3/2)u_n$ for accretion Mach numbers, $2 \leq M_0 \leq 100$. However, as CR pressure builds in the shock precursor, the total compression through the shock increases, and the shock slows down. That is, the *instantaneous* shock speed, $u'_s(t)$, relative to the accretion flow decreases over time. In addition, the gas subshock weakens as the flow is decelerated and heated in the precursor by the CR pressure gradient.

We ran most simulations until time $t_f/t_n = 20 - 40$, which is generally sufficient to reach an approximate dynamical steady state, as discussed in §3. Several much longer simulations based on a new “coarse grained momentum finite volume” code in development have also been carried out to confirm the time asymptotic behaviors, as discussed in §3.5. The simulated space is $x/x_n = [0, 20]$ for $t_f/t_n = 20$ and $x/x_n = [0, 40]$ for $t_f/t_n = 40$ with $N = (1 - 2) \times 10^4$ spatial zones on the base grid. The simulations were carried out on a base grid with $\Delta x_0 = (2 - 4) \times 10^{-3}$ using $l_{\max} = 7$ additional grid levels with a refinement of two, so $\Delta x_7 = \Delta x_0/2^7$ at the finest grid level. The number of refined zones around the shock is $N_{rf} = 50$ on the base grid and so there are $2N_{rf} = 100$ zones on each refined level. To avoid technical difficulties the AMR technique is turned on and the CR injection and acceleration are activated only after the shock propagates to a half length of the pre-defined AMR refinement region in the base grid. This initial delay of the CR injection and acceleration should not affect the final outcomes. For all models we use 230 uniformly spaced logarithmic momentum zones in the interval $\log(p/m_p c) = [\log p_0, \log p_1] = [-3.0, +3.0]$

Shocks formed by steady accretion flow onto cosmic structure pancakes provide a convenient prototype of our modeled shocks. We, therefore, refer to the upstream flows as “accretion flows”, and specify the flow speed and Mach number with respect to the reflecting symmetry plane. The models are also applicable to other cosmic structure shocks associated with filaments, knots and individual clusters. In Kang and Jones (2002) we considered a set of models with fixed infall speed, $u_0 = -1500 \text{ km s}^{-1}$ (“constant u_0 ” models), while the preshock temperature was varied according to $T_0 = 10^4 \text{K}(100/M_0)^2$ with $2 \leq M_0 \leq 100$. In Kang (2003), on the other hand, we set the preshock temperature at $T_0 = 10^4 \text{ K}$ (“constant T_0 ” models), and varied the shock speeds according to $u_0 = (-15 \text{ km s}^{-1})M_0$, with $5 \leq M_0 \leq 50$. We now extend the study of Kang (2003) to include higher preshock temperatures, and also to include the effects of pre-existing CRs in the shock evolution. In particular we include: 1) $T_0 = 10^6 \text{ K}$ shocks without pre-existing CRs, 2) $T_0 = 10^4 \text{ K}$ shocks with pre-existing CRs, and 3) $T_0 = 10^6 \text{ K}$ shocks with pre-existing CRs. For $T_0 = 10^4 \text{ K}$ upstream conditions models with $5 \leq M_0 \leq 5$ ($75 \text{ km s}^{-1} \leq u_n \leq 750 \text{ km s}^{-1}$) are considered, while for $T_0 = 10^6 \text{K}$ conditions we include cases with $2 \leq M_0 \leq 50$ ($300 \text{ km s}^{-1} \leq u_n \leq 7500 \text{ km s}^{-1}$).

We note, for $T_0 = 10^6$ K conditions, models with $M_0 \leq 20$ ($u_n \leq 3000$ km s $^{-1}$) would be relevant for cosmic structure shocks, but models with $M_0 = 30$ and 50 are included to explore the similarity issue discussed above in §2.4. In determining these sets of model parameters, we considered the following factors. In astrophysical environments photoionized gas of 10^4 K is quite common. For example, Ly α clouds and the intergalactic medium in cosmological sheets and voids are believed to be photoionized during the reionization epoch (Loeb and Barkana 2002). Also the preshock gas can be photoionized and heated to $\sim 10^4$ K by the diffuse radiation emitted by hot postshock gas when $u_s \gtrsim 110$ km s $^{-1}$ (Shull and McKee 1979; Kang and Shapiro 1992; Draine and McKee 1993). On the other hand, hot and ionized gas of $> 10^6$ K is also found in the hot phase of the ISM (McKee and Ostriker 1977; Spitzer 1990) and in the intracluster medium of X-ray clusters (Fabian 1994).

Since cosmological simulations indicate that most diffuse plasma in large scale cosmic structures is likely to be shocked more than once during structure formation, it is likely that many “internal shocks” process plasma that carries previously accelerated CRs. We, therefore, include shock simulations including these populations. For pre-existing, upstream CRs we assumed a simple power-law spectrum smoothly connected to the upstream thermal Maxwellian distribution (f_M) at a momentum p_M as

$$f_{up}(p) = f_M(p_M)(p/p_M)^{-q_{in}} \quad (4)$$

for $p_M < p < p_1$, where $p_M = 5(m_p k_B T_0)^{1/2}$, $p_1 = 10^3$. For $T_0 = 10^4$ K shocks we considered in the pre-existing CR cases an upstream CR pressure condition, $P_{c,0} = 0.25P_{g,0}$, using $q_{in} = 4.7$. For $T_0 = 10^6$ K shocks we included three different upstream conditions; namely, $P_{c,0} = 0.25P_{g,0}$ ($q_{in} = 4.5$), $P_{c,0} = 0.5P_{g,0}$ ($q_{in} = 4.4$) and $P_{c,0} = P_{g,0}$ ($q_{in} = 4.3$). The CR spectral forms represent test-particle populations for previous shocks with moderate Mach numbers in the range, $2.5 \lesssim M_s \lesssim 4$. Table 1 provides a summary of the new models computed for the present study.

2.6. Injection and Acceleration Efficiencies

It is useful to characterize the efficiency with which low energy CRs are injected at the shocks. We define the injection efficiency as the fraction of particles that have entered the shock from far upstream and then injected into the CR distribution:

$$\xi(t) = \frac{\int_0^{x_{max}} dx \int_{p_{inj}}^{p_1} 4\pi f_{CR}(p, x, t) p^2 dp}{\int_{t_i}^t n_0 u'_s(t') dt'} \quad (5)$$

where f_{CR} is the CR distribution function, n_0 is the particle number density far upstream, and t_i is the time when the CR injection/acceleration is turned on ($t_i \approx 3t_n$ for $M_0 \geq 5$ and

$t_i \approx 2t_n$ for $M_0 = 2$).

If the subshock speed becomes steady, then $n_0 u'_s$ is the same as the particle flux swept by the subshock, $n_1 u_{\text{sub}}$, where n_1 is the particle number density immediately upstream of the subshock. However, in our simulations these two flux measures can differ by up to 10% for strong shock models, because the shock speed is changing slowly.

As a measure of efficiency of CR energy extraction at shocks, we define the “CR energy ratio”, Φ ; namely, the ratio of the total CR energy within the simulation box to the kinetic energy in the *initial shock frame* that has entered the simulation box from far upstream,

$$\Phi(t) = \frac{\int_0^{x_{max}} dx E_{\text{CR}}(x, t)}{0.5\rho_0(u'_{s,0})^3 t}. \quad (6)$$

All shock models have the same normalized upstream mass density and velocity, ρ_0 and u_0 , but different upstream gas thermal energy density, $P_{g,0}/(\gamma_g - 1)$, depending on M_0 . Therefore, we use the kinetic energy flux rather than the total energy flux to normalize the “CR energy ratio”. Alternatively, the ratio defined with the total energy flux, $F_{\text{tot}} = u'_{s,0}[0.5\rho_0(u'_{s,0})^2 + \gamma_g P_{g,0}/(\gamma_g - 1) + \gamma_{c,0} P_{c,0}/(\gamma_{c,0} - 1)]$, can be calculated from the following relation,

$$\Phi_{\text{tot}}(t) \approx \frac{\Phi(t)}{1 + \frac{3}{M_0^2} \left(\frac{u_0}{u'_{s,0}}\right)^2 (1 + P_{c,0}/P_{g,0})}, \quad (7)$$

where we assume $\gamma_{c,0} \approx 5/3$ for the preshock CR population. This shows that $\Phi_{\text{tot}} \approx \Phi$ for large values of M_0 , while $\Phi_{\text{tot}} \approx (3/5)\Phi$ for $M_0 = 2$ and $P_{c,0} = P_{g,0}$.

3. Simulation Results

We can define three key stages of shock evolution in response to CR feedback: 1) Development of the shock precursor that slows and heats the flow entering the gas subshock, reducing the Mach number of the latter; 2) achievement of an *approximately* time-asymptotic dynamical shock transition, including nearly steady postshock CR and gas pressures; 3) continued, approximately “self-similar” evolution of the shock structure for Bohm-type diffusion, as CRs are accelerated to ever higher momenta. Once stage (3) is reached, there is little change in the dynamical properties of the shocks, and, in particular, little change in the total efficiency with which kinetic energy is transferred to CRs. Thus, given the rapidly increasing computational cost to simulate acceleration of CRs to still higher energies with Bohm diffusion (which more than quadruples for each factor of two increase in maximum CR momentum), we deemed it sufficient to the questions being addressed to terminate the simulations at the times indicated.

As Kang (2003) showed, the evolution of CR modified shocks with Bohm-type diffusion are mainly determined by the shock Mach number for a given injection parameter. This includes the efficiency of energy transfer to CRs, Φ . That is, two shocks with the same Mach number, but with different shock speeds evolve qualitatively similarly when expressed in terms of characteristic diffusion scales, t_n and x_n . During the early evolutionary stage, however, the similarity between the two shocks may break down as pointed out in §2.4. As described there, this happens if the shock speed is larger than a percent or so of the speed of light, on account of the different momentum-velocity scalings for nonrelativistic and relativistic particles at injection. As a result, the ratio of $P_c/(\rho_n u_n^2)$ increases faster and nonlinear modification sets in earlier in terms of t/t_n in the shock with lower speed. Thus, depending on when the transition from nonrelativistic to relativistic population occurs, early evolution of the two shocks can be different (*e.g.*, see $M_0 = 30$ models in figure 2), although they still eventually approach similar time-asymptotic states.

The other factor that can affect the similarity is the presence of pre-existing CRs. For strong shocks of $M_s > 10$, the preshock CR pressure is only a few percent of the total energy flux even when $P_c \sim P_g$ far upstream. In those cases the presence of pre-existing CRs is effectively equivalent to having a slightly higher injection rate (*i.e.*, larger ϵ), which speeds up the initial shock evolution. For strong shocks, our previous studies have shown that the time asymptotic CR acceleration efficiency depends only weakly on the injection rate (Kang, Jones, and Gieseler 2002; Kang and Jones 2002), provided the injection remains above a minimum threshold for “efficient” DSA (see also, *e.g.*, Berezhko et al. 1996). On the other hand, for weak shocks, a pre-existing CR pressure comparable to the upstream gas pressure represents a significant fraction of the total energy entering the shock, so pre-existing CRs have far more impact. Also the time asymptotic CR acceleration efficiency in weak shocks depends sensitively on the injection rate and increases with ϵ . Hence we should expect that relatively weak CR shocks ($M_s < 5$) will be substantially altered by the presence of a finite upstream P_c .

3.1. Evolution of Shock Structures

Figure 1 compares the time evolution of two CR modified shock models with accretion Mach number $M_0 = 5$, but with different physical flow speeds and upstream CR conditions. The light lines show the flow model with $T_0 = 10^4$ K and the pre-existing CR population, $f_{up} \propto p^{-4.5}$, while the heavy lines show the model with $T_0 = 10^6$ K and $f_{up} \propto p^{-4.7}$. The pressure due to the pre-existing CR particles is $P_{c,0} = 0.25P_{g,0}$ in both models. Note that the physical time and length scales are different, since $t_n \propto u_n^{-2}$ and $x_n \propto u_n^{-1}$ ($u_n = 75 \text{ km s}^{-1}$

for $T_0 = 10^4$ K models and $u_n = 750$ km s $^{-1}$ for $T_0 = 10^6$ K models).

In the model with $u_n = 75$ km s $^{-1}$ CR particles are injected at much lower injection momenta. Since for a fixed Mach number their initial acceleration times scale as $\tau_{acc}/t_n \propto p_{inj}^2$, the acceleration and shock modification takes place more rapidly in these time units compared to the model with $u_n = 750$ km s $^{-1}$. The value of $P_c/(\rho_n u_n^2)$ approaches 0.8 for the model with $u_n = 75$ km s $^{-1}$, while it approaches 0.65 for the model with $u_n = 750$ km s $^{-1}$. Otherwise, the overall evolution is roughly similar.

Figure 2 shows that even for much higher Mach numbers, $M_0 = 30$, two shocks with $u_n = 450$ km s $^{-1}$ and $u_n = 4500$ km s $^{-1}$ approach similar time-asymptotic states, although their early evolutions are very different. However, as the shock speed increases further, substantial differences develop in the early evolution. For $M_0 = 50$ models, for example, unlike the shocks shown in the figures, the overall shock structures then evolve much more slowly in our normalized time units, since the injection momentum is no longer nonrelativistic. Then the Bohm-like diffusion coefficient and the CR partial pressure near this momentum do not scale with p^2 as they do for nonrelativistic momenta. The approximate self-similarity of the shock evolution breaks down under those conditions. Even those shocks, however, do approach similar time asymptotic states for a given Mach number.

The flow entering the piston is decelerated first by the precursor and then by the subshock in our simulation. For a pure gas fluid with a constant adiabatic index, the postshock flow speed relative to the piston should be uniformly zero. This should be approximately true for the models with inefficient CR acceleration in our simulations (see, for example, Fig.4 below). In CR modified shocks, however, the “effective” adiabatic index decreases due to increasing CR energy, so the total compression through the shock increases and the shock slows down over time. This transition in the compressibility of the flow leads to a net forward flow velocity of $0.04 < u/u_n < 0.07$ in the piston rest frame for the two models shown in Figs. 1 and 2. However, the net flow speed is decelerated by the positive gradient of the combined postshock pressure ($P_c + P_g$) and approaches a smaller value ($0.02 < u/u_n < 0.03$) at the terminal simulation time.

As noted in previous *time-dependent* studies (see the references in §1), the compression factor for these CR dominated shocks relaxes to values still higher than that for a gasdynamic shock, even a for a fully relativistic gas, even though energy is not leaving the system in our simulations. The reason has to do with the *evolving* distribution of energy in the system. In particular, for a diffusion coefficient increasing with p , especially for high Mach number, CR dominated shocks, the compression factor can remain much higher than what is expected in a steady-state, energy-conserving shock jump for relativistic gas (*i.e.*, $\rho_2/rho_0 = 7$). This is because energy is being continuously transported out of the region of the subshock by

diffusion of the highest energy CRs with an ever-increasing diffusion scale $x_d(p_{\max})$. More extensive discussion can be found in Kang, Jones, and Gieseler (2002).

3.2. Effect of Pre-existing CRs for Weak Shocks

Figure 3 compares the evolution of shocks *with* and *without* pre-existing, upstream CRs. Four sets of shocks are illustrated: 1) $M_0 = 5$, $u_n = 75 \text{ km s}^{-1}$, and $T_0 = 10^4 \text{ K}$ (upper left panel), 2) $M_0 = 5$, $u_n = 750 \text{ km s}^{-1}$, and $T_0 = 10^6 \text{ K}$ (upper right panel), 3) $M_0 = 30$, $u_n = 450 \text{ km s}^{-1}$, and $T_0 = 10^4 \text{ K}$ (lower left panel), and 4) $M_0 = 30$, $u_n = 4500 \text{ km s}^{-1}$, and $T_0 = 10^6 \text{ K}$ (lower right panel). The approximate self-similarity for the evolution of these shocks, when described in normalized units is apparent. In addition one can see that the presence of pre-existing CRs is clearly more important for low Mach number shocks.

It is especially important to consider the influence of pre-existing CRs in low Mach number shocks, since internal shocks with $M_s \sim 3$ may be the most important for dissipation in shock-heated gas inside nonlinear structures (Ryu et al. 2003). We already know that CR acceleration efficiency in low to moderate strength shocks depends sensitively on the injection rate and increases with ϵ (Kang and Jones 2002). Our new simulations show that the CR acceleration efficiency in these shocks depends similarly on the pre-existing (upstream) CR pressure. That trend was apparent in figure 1. Figure 4 emphasizes the point impressively for even lower Mach number shocks. It shows the time evolution of the models with accretion flow Mach number $M_0 = 2$ and $u_0 = -300 \text{ km s}^{-1}$, which drive shocks with initial Mach number of $M_s = 3$ into the preshock gas with $T_0 = 10^6 \text{ K}$. Three models are compared in the figure: 1) a model with no pre-existing CRs (solid lines), 2) a model with $P_{c,0} = 0.25P_{g,0}$ (dotted lines), and 3) a model with $P_{c,0} = 0.5P_{g,0}$ (dashed line). For the model without the pre-existing CRs and with injection parameter, $\epsilon = 0.2$, the CR injection is small and the resulting CR acceleration is inefficient. The solution is essentially a test-particle solution, with minimal CR modifications to the flow structure. There are a couple of related reasons for the impact of the upstream CRs in the two other models. First, the pressure of the pre-existing CRs cannot be neglected in the shock transition compared to the total shock energy flux. In addition, the inflowing CRs act like a large source of injected CRs, effectively enhancing the injection rate (see also Blasi 2003). Kang and Jones (2002) also considered similar $M_0 = 2$ models without the pre-existing CRs ($u_0 = -1500 \text{ km s}^{-1}$, and $T_0 = 2.5 \times 10^7 \text{ K}$), but with a range of injection parameters, $\epsilon = 0.2 - 0.4$. We found that the postshock CR pressure increased over this range of ϵ from $P_c = 0.04$ to $P_c = 0.24$, while the associated injection rate rose from $\xi = 10^{-4}$ to $\xi = 10^{-2}$ (see figure 8 in Kang and Jones 2002). These results imply that even in low Mach number shocks the CR acceleration can have significant

dynamical influences, when the injection rate is as high as $\xi \sim 10^{-2}$ or when the upstream CR pressure is greater than a few times 10 % of the gas pressure. This could be important in the context of cosmic structure shocks, especially for “internal shocks” in which the upstream plasma already carried a significant population of CRs produced in an earlier era.

3.3. The Particle Distribution

Time evolution of the distribution function $g(p) = f(p)p^4$ at the gas subshock is shown in figure 5 for the models with $T_0 = 10^6$ K and with $f_{up} \propto p^{-4.5}$. The dotted line shows the initial Maxwellian distribution with T_0 and the specified power-law distribution for the pre-existing CR population. The postshock thermal distribution during the early evolution (before shock modification) should have $T_2 \propto M_0^2$, so the injection momentum, $p_{inj} \propto M_0$ for $t/t_n < 1$. However, as energy transfer to CRs increases over time and the gas subshock weakens, the peak in the Maxwellian distribution shifts to lower momenta. The model with $M_0 = 30$ shows this effect clearly. This nonlinear feedback is greater for higher Mach number, so that the postshock temperature of evolved CR modified shocks depends on M_0 much more weakly than the standard M_0^2 .

It is useful to identify p_{max} as the momentum above which $g(p)$ drops sharply, characterizing the effective upper cutoff in the CR distribution, at a given time since shock formation. This momentum is generally easily identified. We find that it is approximately related to the age of the shock as $p_{max} \sim 0.4(t/t_n)$ for $p_{max} > 1$. This explains why values of p_{max} are similar at a given value of t/t_n for all models considered here, independent of u_n , injection momentum, or shock Mach number. The previously described back reaction of the CRs on the gas subshock acts to move the shock towards a limiting form and postshock state. On the one hand, a fraction of CR particles injected at early times continues being accelerated to higher momenta, so that $p_{max}(t)$ always increases until they are subject to escape due to geometry or insufficient scattering. On the other hand, particle injection becomes less efficient as the subshock feature weakens. Because of this reduced source spatial diffusion causes the number density of CRs near the subshock at a given momentum to decrease with time for any $p < p_{max}(t)$. Combined, these effects cause the postshock CR pressure, P_c , to approach a time-asymptotic value, and, for Bohm-like diffusion, the shock structure to become approximately self-similar.

3.4. Cosmic Ray Injection and Acceleration Efficiencies

Figure 6 illustrates the time averaged injection efficiency, $\xi(t)$, defined by equation (9) for models without pre-existing CRs. The calculated injection efficiency ranges from \sim a few $\times 10^{-5}$ to $\sim 10^{-3}$, depending on the subshock Mach number, the shock speed, and the injection parameter, ϵ . As outlined in §2.4 and discussed fully in Kang, Jones, and Gieseler (2002), the modeled thermal-leakage injection process is less efficient for weaker subshocks and for smaller ϵ (stronger wave trapping of suprathermal particles in the postshock environment). Injection is also less efficient for lower shock speeds, because the diffusive flux of injected particles crossing the subshock is smaller for smaller injection momentum ($p_{\text{inj}} \propto u_s$). So, for a given Mach number the models with higher shock speed (*i.e.*, higher T_0 in figure 6) have larger values of $\xi(t)$. For strong shocks the subshock weakens significantly due to the CR nonlinear feedback, so the injection efficiency slowly decreases over time.

Figure 7 shows for the models with $T_0 = 10^4\text{K}$ the CR energy ratio, Φ , the CR pressure and the gas pressure at the subshock normalized by the far upstream ram pressure in the *initial* shock frame, *i.e.*, $P_{c,2}/(\rho_0 u'_{s,0}{}^2)$, and $P_{g,2}/(\rho_0 u'_{s,0}{}^2)$. In addition the bottom panels show the CR pressure normalized by the far upstream ram pressure in the *instantaneous* shock frame, $P_{c,2}/(\rho_0 u'_s{}^2)$. The left panels illustrate the models without pre-existing CRs, while right panels show the models with $P_{c,0} = 0.25P_{g,0}$. As described in the previous subsection, the postshock P_c for all Mach numbers increases until a balance between injection/acceleration and advection/diffusion of CRs is achieved. After that time, which corresponds in these simulations to the generation of moderately relativistic CRs in the shock, the postshock CR pressure remains almost steady. Simultaneously, the CR energy ratio, Φ , also initially increases with time, but then asymptotes to a constant value, once $P_{c,2}$ has reached a quasi-steady value. The asymptotic values result from the “self-similar” behavior of the P_c distribution. Since both the numerator and denominator in equation (6) increase approximately linearly with time in the case of the self-similar evolution of E_c , Φ becomes steady when $P_{c,2}$ becomes constant. As illustrated in Figure 7, time-asymptotic values of Φ increase with the accretion Mach number M_0 , approaching $\Phi \approx 0.5$ for $M_0 > 20$ by the simulation termination times. As expected from the discussion in §3.4, the presence of pre-existing CRs increases the asymptotic postshock P_c for the weaker shock, $M_0 = 5$ model, while it does not affect the strong shock models with $M_0 \geq 10$. Figure 7 also illustrates the well-known result that strong shocks can be mediated mostly by CRs while the postshock gas thermal energy is reduced greatly compared to that in conventional gasdynamic shocks of the same Mach number. As a result of nonlinear feedback the shock slows down and so the ratio of $P_{c,2}/(\rho_0 u'_s{}^2)$ can reach ~ 0.9 , while the ratio of $P_{c,2}/(\rho_0 u'_{s,0}{}^2)$ reaches ~ 0.6 in these models.

In figure 8 we present the same quantities for the models with $T_0 = 10^6$ K. As explained in the previous section, due to the higher injection momenta, the CR acceleration is slower to develop for the models with $M_0 \geq 20$, compared to the same Mach number model with lower shock speed. Especially for the $M_0 = 50$ model, the postshock P_c continues to increase at the termination time ($t/t_o = 40$) of the simulation. Again, the presence of pre-existing CRs significantly increases the postshock P_c at low Mach number models ($M_0 \leq 5$). We show the same quantities for low Mach number simulations with even higher pre-existing P_c in figure 9. We see that the postshock P_c increases with the pre-existing P_c for these low Mach number models.

3.5. Time Asymptotic Behaviors

As discussed above, some characteristics of the CR modified shocks seem to have reached quasi-steady states well before the termination time for most of the models considered in this work. We have further explored these time asymptotic behaviors by performing much longer simulations with a new “Coarse-Grained Momentum Finite Volume” (CGM) numerical scheme under development. CGM utilizes the fact that the distribution function can be approximated as a piecewise power-law within a given broad momentum bin and so only roughly one momentum bin per octave is necessary to follow the CR population numerically. Details and tests of the CGM numerical method will be presented in a forthcoming paper (Jones and Kang 2004). In figures 10 and 11, we show the simulation results of $M_0 = 5$ and $M_0 = 30$ models, respectively, which were calculated by this CGM method up to $t/t_n = 1000$. No pre-existing CRs were assumed and 14 momentum bins were used for these calculations. The heavy solid lines are for the simulation results at $t/t_n = 20$ for the $M_0 = 5$ model and $t/t_n = 40$ for the $M_0 = 30$ model which were calculated by the “fine-grained momentum” method described in §2 and used for all the other results presented in this paper. Those simulations were carried out with 240 momentum bins. These figures confirm very firmly the aforementioned “self-similarity” of the shock evolution and the time-asymptotic behaviors.

Thus we show in figure 12 values of the CR energy ratio Φ at the termination time as a function of the initial unmodified shock Mach number, M_s , as a simple measure of the CR acceleration efficiency. For convenience in comparing with other plots Values of M_s are listed against M_0 in Table 1. Flows with $T_0 = 10^4$ are shown in the upper panel, while shocks developed in $T_0 = 10^6$ flows are represented in the lower panel. For comparison, we also plotted in the upper panel results from “constant u_0 ” models with $u_0 = -1500$ km s⁻¹ and $T_0 = 10^4(100/M_0)^2$ K, originally presented in figure 7 of Kang (2003). Those models, which did not include a pre-existing CR population, behave similarly to the new models

considered in the present work. In each series of simulations the efficiency asymptotes to $\Phi \approx 0.5$ for large M_s . This asymptotic efficiency is independent of $P_{c,0}/P_{g,0}$; *i.e.*, the level of pre-existing CRs. It also reflects the fact that the postshock CR pressures in the high Mach number shocks evolve in all cases roughly to 60% of the inflowing ram pressure measured in the initial shock rest frame, $\rho_0 u_{s,0}'^2$. In weak to moderate strength shocks, on the other hand, the CR efficiencies shown in figure 12, or the postshock CR pressures illustrated in figures 7 and 8, depend strongly on $P_{c,0}/P_{g,0}$. A rough dividing line for these two behavior domains is $M_s \sim 20$. For the $M_s = 3$ model without the pre-existing CRs and $\epsilon = 0.2$, the injection rate $\xi \approx 2 \times 10^{-5}$ and Φ approaches to only 0.04. Since $0.3 \lesssim \epsilon \lesssim 0.4$ is indicated for strong shocks (Malkov and Völk 1998) and weaker wave fields are expected in lower Mach shocks, leading to larger values of ϵ , we show three addition models for $\epsilon = 0.25, 0.3$, and 0.4 with $M_s = 3$, $T_0 = 2.5 \times 10^7 \text{K}$ and no pre-existing CRs, originally presented in figure 8 of Kang and Jones (2002), in the upper panel of figure 12. In Ryu et al. (2003) the CR efficiency model, $\Phi(M_s)$, for $\epsilon = 0.3$ was adopted in the calculation of the CR energy generated by cosmic structure shocks. We note that the functional minimum in $\Phi(M_s)$ for the models with pre-existing CRs is an artifact of the definition of Φ , which is normalized by the inflowing kinetic energy, not the total energy. The thermal energy flux is a significant fraction of the kinetic energy flux for low Mach number shocks. There is no minimum in the function Φ_{tot} , as defined in equation 7. For instance the value $\Phi(M_s = 3) \approx 0.67$ shown in figure 12, becomes $\Phi_{tot}(M_s = 3) \approx 0.4$.

As also pointed out in §3.2, the increases in CR energy ratio for weak shocks when they process plasma that contains pre-existing CRs, could be important to understanding the properties of cosmic structure formation shocks. In addition, most baryonic matter in clusters has been shocked more than once before the current epoch (Ryu et al. 2003). This means that many of the shocks primarily responsible for energy dissipation during structure formation may be influenced by CRs accelerated in previous shock events, since magnetic field strengths at levels discussed in the introduction should tie CRs up to moderately relativistic energies to the thermal plasma over cosmic time scales (*e.g.*, Völk, Aharonian & Breitschwerdt 1996). In that case, those shocks may be substantially more efficient at CR acceleration than one might otherwise expect.

4. Summary

Energy dissipation at collisionless shocks involves complex physical processes and plays crucial roles in the evolution of shock-heated astrophysical plasmas. Here our focus is CR acceleration via the first-order Fermi process at cosmic shocks that form in and around

nonlinear structures during the formation of large scale structure in the universe. Using our cosmic-ray AMR Shock code (Kang, Jones, and Gieseler 2002), we have calculated the CR acceleration at 1D quasi-parallel shocks driven by plane-parallel infall flows with $|u_0| = 75 - 7500 \text{ km s}^{-1}$ and preshock temperatures of $T_0 = 10^4 - 10^{7.6} \text{ K}$. Mach numbers of the resulting shocks range over $2 \leq M_s \leq 133$, which covers the characteristic shock Mach numbers found in cosmological hydrodynamic simulations of a Λ CDM universe (Ryu et al. 2003).

The main purpose of this study is to explore how the CR acceleration efficiency at cosmic structure shocks depends on the preshock temperature, shock speed and pre-existing CRs as well as shock Mach number. This, in turn, affects the thermal and dynamical history of the shocked-heated baryon gas, since the energy transfer to CRs reduces the thermal energy of the gas and increases the compressibility of the gas flow, much like radiative shocks.

Unlike pure gasdynamic shocks, downstream states of the CR modified shocks cannot be found from "shock jump conditions", so they have to be integrated time-dependently from given initial states or found from nonlinear analytical methods. Time-dependent simulations are computationally expensive, because the CR diffusion and acceleration processes contain a wide range of length and time scales. Fortunately, there are approximate similarity properties that can be employed to study the time asymptotic behavior of evolved CR modified shocks when they are mediated by Bohm-like diffusion. Firstly, the CR pressure approaches a steady-state value in a time scale comparable to the acceleration time scales for mildly relativistic protons after which the evolution of CR modified shocks becomes approximately "self-similar". This feature enables us to predict time asymptotic values of the CR acceleration efficiency, although we followed the CR acceleration up to only moderately relativistic energies (*i.e.*, $p_{\text{max}}/(mc) \sim 16$). We have confirmed these time asymptotic behaviors through much longer simulations with a new, more efficient, numerical scheme (Jones and Kang 2004), which were extended to achieve the cut-off momentum $p_{\text{max}}/(mc) \sim 400$. Secondly, *two models with the same Mach number, but with different accretion speeds* show qualitatively similar evolution and structure when the dynamical evolution is presented in terms of characteristic diffusion scales, $t_n = \kappa_n/u_n^2$ and $x_n = \kappa_n/u_n$. Such similarities are only approximate, however, because the partial CR pressure and the Bohm diffusion coefficient for transrelativistic CRs do depend on the momentum $m_p c$. Since the effective injection momentum is $p_{\text{inj}}/m_p c \propto (u_s/c)$, the initial evolution depends on the shock speed as well as Mach number.

Finally, we state the main conclusions of our study, which can be summarized as follows:

1) Suprathermal particles can be injected efficiently into the CR population at quasi-parallel cosmic shocks via the thermal leakage process. For a given injection parameter

defined in the text, ϵ , the fraction of injected CRs increases with the subshock Mach number, but approaches $\xi \sim 10^{-3}$ in the strong shock limit.

2) For a given value of ϵ , the acceleration efficiency increases with the shock Mach number, but approaches a similar value in the strong shock limit. Time asymptotic values of the ratio of CR energy to inflowing kinetic energy, Φ , converge to $\Phi \approx 0.5$ for $M_s \gtrsim 30$ and it is relatively independent of other upstream or injection parameters (see figure 12). Thus, strong cosmic shocks can be mediated mostly by CRs and the gas thermal energy can be up to ~ 10 times smaller than that expected for gasdynamic shocks.

3) For weak shocks, on the other hand, the acceleration efficiency increases with the injection rate (or ϵ) and the pre-existing P_c (see figure 12). For cosmologically common $M_s = 3$ shocks, for example, $\Phi \sim 0.04$ for $\epsilon = 0.2$ and $\Phi \sim 0.2$ for $\epsilon = 0.3$ in the absence of pre-existing CRs. The presence of a pre-existing CR population acts effectively as a higher injection rate than the thermal leakage alone, leading to greatly enhanced CR acceleration efficiency in low Mach number shocks. We found even for weak shocks of $M_s = 3$, that up to 40 % of the total energy flux through the shocks can be transferred to CRs, when the upstream CR pressure is comparable to the gas pressure in the preshock flow.

HK was supported by KOSEF through Astrophysical Research Center for the Structure and Evolution of Cosmos (ARCSEC) and grant-R01-1999-00023 and by Pusan National University Research Grant. TWJ is supported by NSF grants AST00-71167 and AST03-07600, by NASA grant NAG5-10774 and by the University of Minnesota Supercomputing Institute.

REFERENCES

- Allen, G. E., Keohane, J.W., Gotthelf, E.V., et al, 1997, ApJ, 487, L97
- Bamba, A., Yamazaki, R, Ueno, M. & Koyama, K. 2003, ApJ.589, 827
- Bell A.R., 1978, MNRAS, 182, 147
- Bell, A.R. and Lucek, S.G. 2001, MNRAS, 321, 433
- Berezhko, E. G., Elshin, & V.Ksenofontov, L. 1996, JETP, 82, 1
- Berezhko, E. G. and Ellison, D. C. 1999, ApJ, 526, 385
- Berezhko E.G., and Völk H.J. 1997, Astroparticle Physics, 7, 183

- Berezhko E.G., and Völk H.J. 2000, A&A357, 283
- Blandford, R. D., and Eichler, D. 1987, Phys. Rept., 154, 1
- Blasi, P. 2003, astro-ph/0310507
- Draine, B. T., and McKee, C. F. 1993, ARAA, 31, 373
- Drury, L. O’C. 1983, Rept. Prog. Phys., 46, 973
- Drury, L. O’C., and Falle, S. A. E. G. 1986, MNRAS, 223, 353
- Ellison, D. C., and Eichler, D. 1985, ApJ, 286, 691
- Ellison, D. C., Baring, M. G. & Jones, F. C. 1995, ApJ, 453, 873
- Fabian, A. C. 1994, ARAA, 32, 277
- Gieseler U.D.J., Jones T.W., and Kang H. 2000, A&A, 364, 911
- Jokipii, R. J. 1982, ApJ, 255, 716
- Jones, T. W. and Kang, H. 2004, in preparation
- Jones, F. C., and Ellison, D. C., 1991, Space Sci. Rev., 58, 259
- Kang, H., 2003, Journal of Korean Astronomical Society, 36, 1
- Kang, H., Jones, T. W. and Ryu, D. 1992, ApJ, 385, 193
- Kang, H., Jones, T. W., LeVeque, R. J., and Shyue, K. M. 2001, ApJ, 550, 737
- Kang, H., & Jones, T. W., 2002, Journal of Korean Astronomical Society, 35, 159
- Kang, H., Jones, T. W., & Gieseler, U.D.J, 2002, ApJ, 579, 337
- Kang, H., and Shapiro, P. R. 1992, ApJ, 386, 432
- Koyama, K. , Petre, R., Gotthelf, E. V. et al. 1995, Nature, 378, 255
- Kulsrud, R. M., Cen, R., Ostriker, J. P. & Ryu, D. 1997, ApJ, 480, 481
- Loeb, A., and Barkana, R. 2002, ARAA, 39, 19
- Kronberg, P. P. 2001, in “High Energy Gamma-Ray Astronomy,” ed: F. Aharonian & H. Völk, AIP Conf. Series, vol 558, p 451

- Lucek, S.G., and Bell, A.R. 2000, MNRAS, 314, 65
- McKee, C. F., and Ostriker, J. P. 1977, ApJ, 218, 148
- Malkov M.A. 1998, Phys. Rev. E, 58, 4911
- Malkov M.A., and Völk H.J. 1998, Adv. Space Res. 21, 551
- Malkov, M. A., Diamond, P. H. & Völk, H. J. 2000, ApJ, 533, L171
- Malkov M.A., and Drury, L.O’C. 2001, Rep. Progr. Phys. 64, 429
- Miniati, F., Ryu, D., Kang, H., Jones, T. W., Cen, R., & Ostriker, J. 2000, ApJ, 542, 608
- Miniati, F., Jones, T. W., Kang, H. & Ryu, D. 2001, ApJ, 562, 233
- Quest K.B., 1988, J. Geophys. Res. 93, 9649
- Ryu, D., Kang, H. & Biermann, P. L. 1998, A&A, 335, 19
- Ryu, D., Kang, H., Hallman, E., & Jones, T. W. 2003, ApJ,
- Schlickeiser, R. & Shukla P. K. 2003, ApJ, 599, L57
- Shull, J. M., and McKee, C. F. 1979, ApJ, 227, 131
- Skilling, J. 1975, MNRAS, 172, 557
- Spitzer, L., 1990, ARAA, 28, 71
- Völk, H. J., Aharonian, F. & Breitschwerdt, D. 1996, S.S.R., 75, 279
- Völk, H. J, Berezhko, E. G. & Ksenofontov, L. T. 2003, A&A, 409, 563

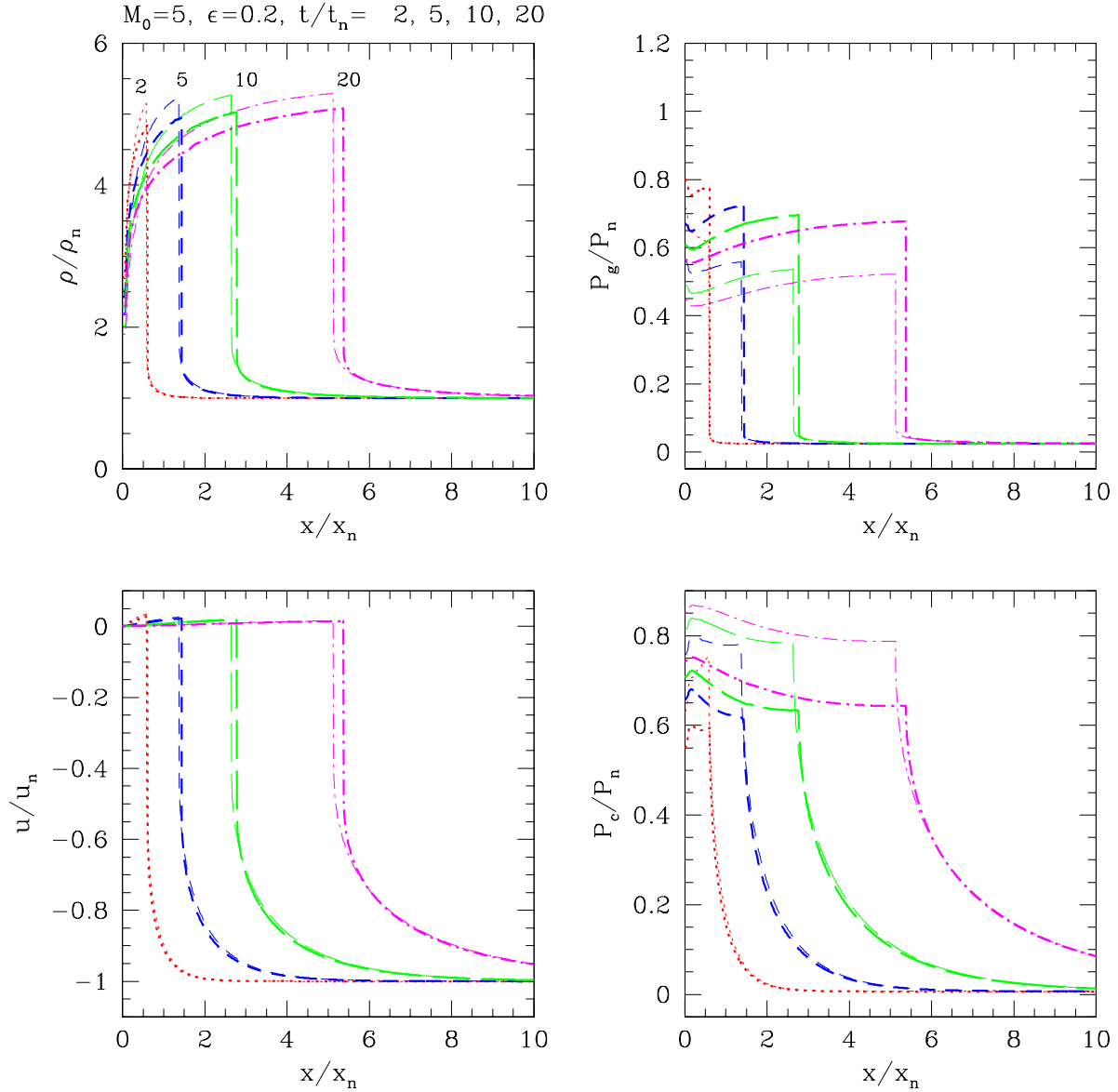


Fig. 1.— Time evolution of the shocks driven by 1D accretion flows with $M_0 = u_n/c_{s,0} = 5$ is shown at normalized times, $t/t_n = 2, 5, 10,$ and 20 . The accretion flow enters from the right boundary ($x/x_n = 20$) and is reflected at the piston ($x/x_n = 0$), leading to a shock with $M_s = 6.8$ propagating to the right. The flow speed is shown in the piston rest frame, so the flow is almost at rest near the piston. The leftmost profile corresponds to the earliest time. Light lines represent a flow with $u_n = 75 \text{ km s}^{-1}$, $T_0 = 10^4 \text{ K}$, and a pre-existing CR population with $f_{up} \propto (p/p_M)^{-4.7}$. Heavy lines represent the model with $u_n = 750 \text{ km s}^{-1}$, $T_0 = 10^6 \text{ K}$, and $f_{up} \propto (p/p_M)^{-4.5}$. For both models the upstream CR pressure is $P_{c,0}/P_{g,0} = 0.25$. The normalization diffusion time scale, $t_n = \kappa_n/u_n^2$, and diffusion length, $x_n = \kappa_n/u_n$ are defined by the accretion speed of each model. The inverse wave-amplitude parameter $\epsilon = 0.2$ is adopted for both models.

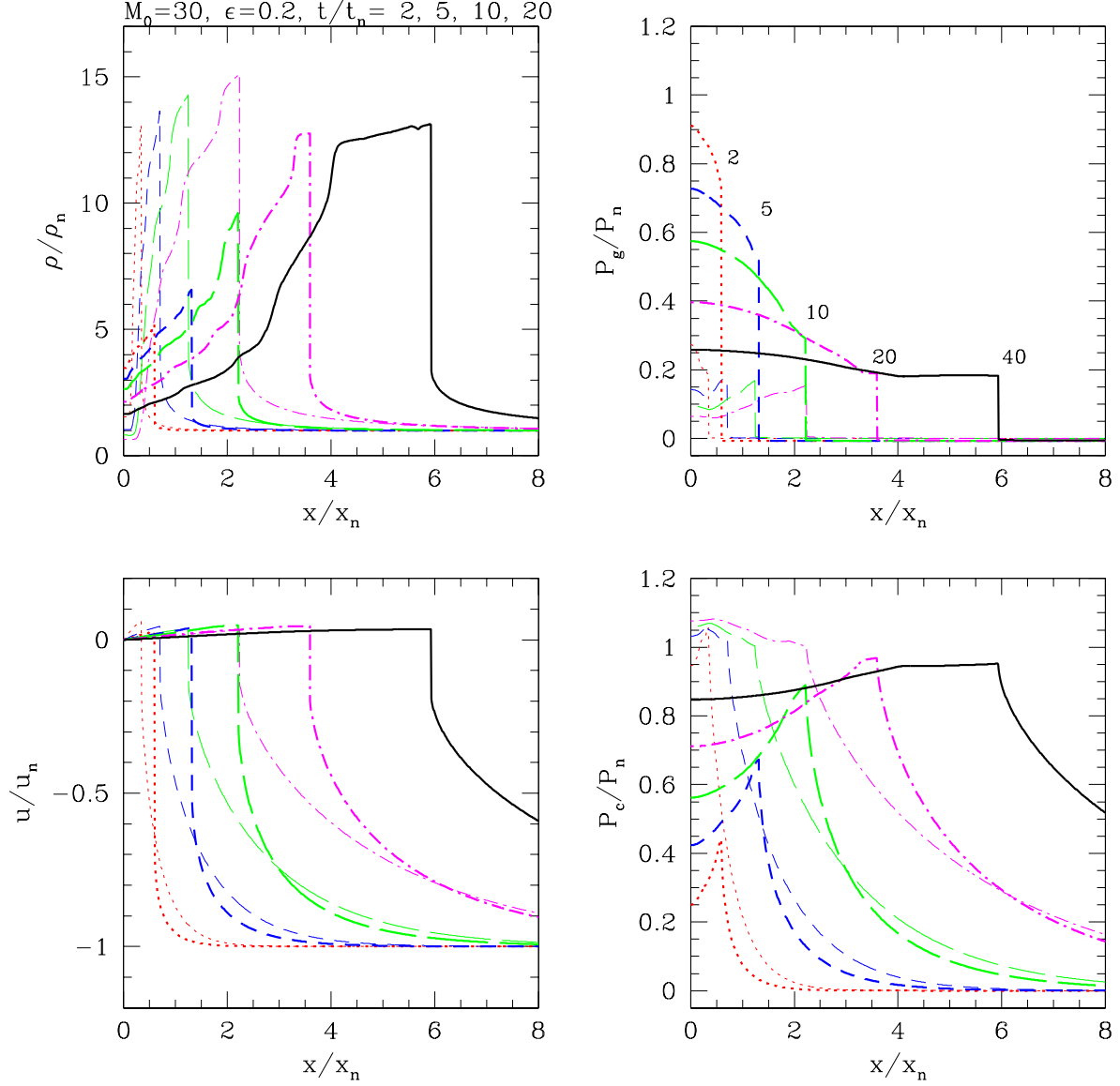


Fig. 2.— Same as Figure 1 except $M_0 = 30$. Light lines are for the model with $u_n = 450 \text{ km s}^{-1}$, $T_0 = 10^4 \text{ K}$, and a pre-existing CR population of $f_{up} \propto (p/p_M)^{-4.7}$, while heavy lines represent the model with $u_n = 4500 \text{ km s}^{-1}$, $T_0 = 10^6 \text{ K}$, and $f_{up} \propto (p/p_M)^{-4.5}$. For both models the upstream CR pressure is $P_{c,0}/P_{g,0} = 0.25$. Note for $T_0 = 10^6 \text{ K}$ model additional curves (heavy solid lines) are shown at $t/t_n = 40$.

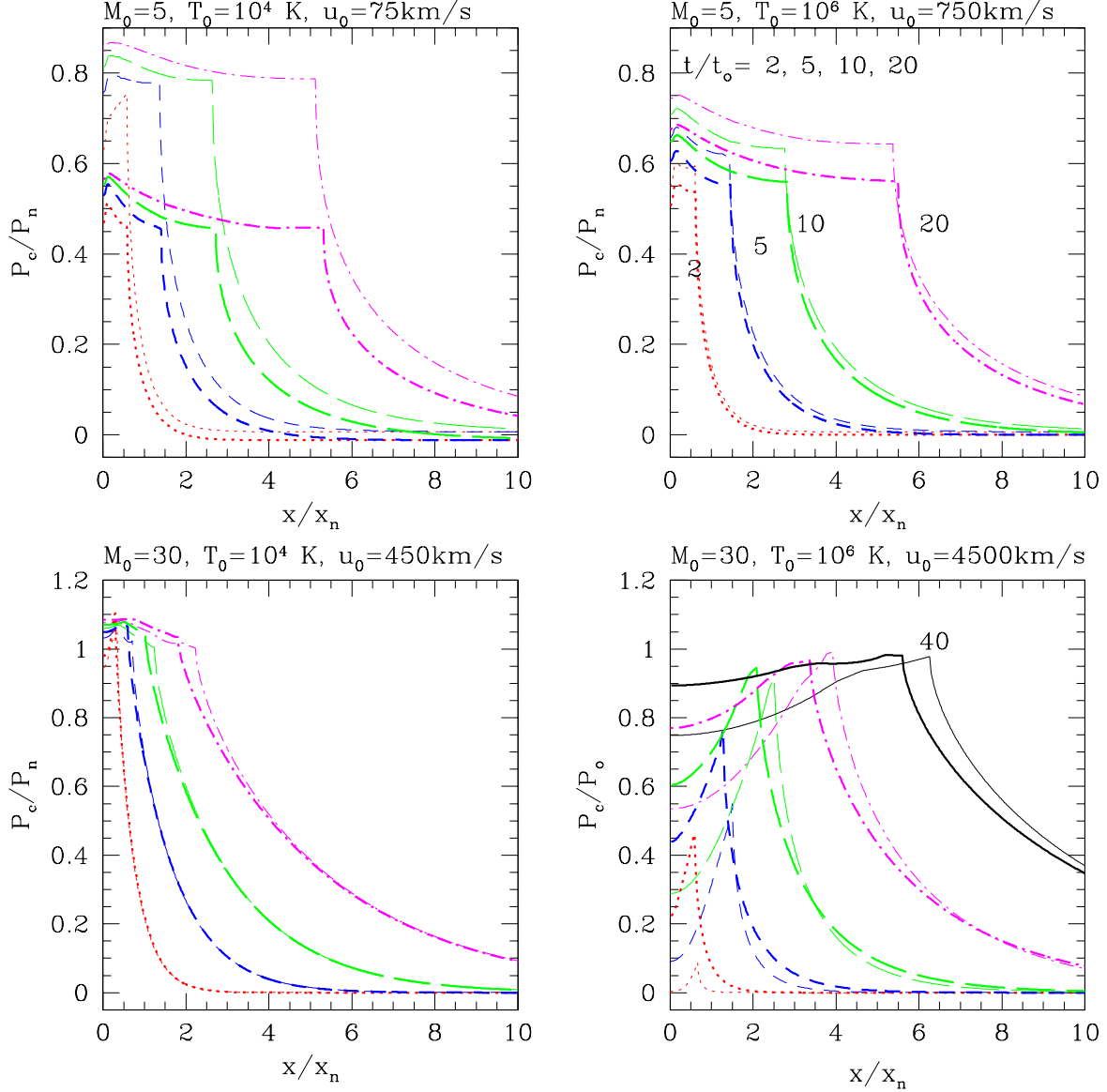


Fig. 3.— Time evolution of the CR pressure for the following models: 1) $M_0 = 5$ and $T_0 = 10^4$ K (upper left panel), 2) $M_0 = 5$ and $T_0 = 10^6$ K (upper right panel), 3) $M_0 = 30$ and $T_0 = 10^4$ K (lower left panel), and 4) $M_0 = 30$ and $T_0 = 10^6$ K (lower right panel). Heavy lines are for the models without pre-existing CRs, while light lines are for the models with $P_{c,0} = 0.25P_{g,0}$.

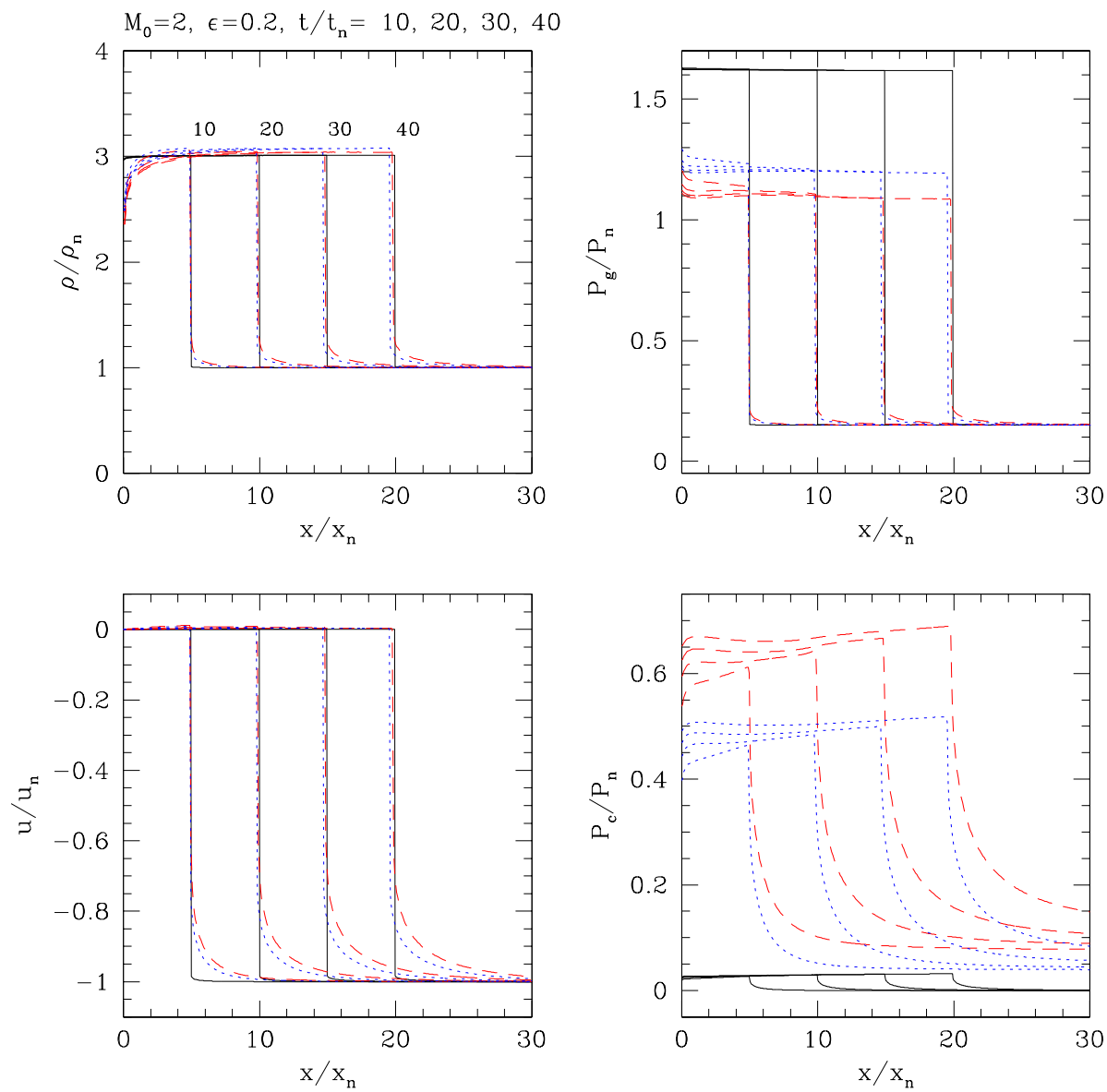


Fig. 4.— Same as Figure 1 except $M_0 = 2$, $T_0 = 10^6\text{K}$ and $u_n = 300 \text{ km s}^{-1}$. The solid lines are for the model with $P_{c,0} = 0.0$, the dotted lines for the model with $P_{c,0} = 0.25P_{g,0}$, and the dashed lines for the model with $P_{c,0} = 0.5P_{g,0}$.

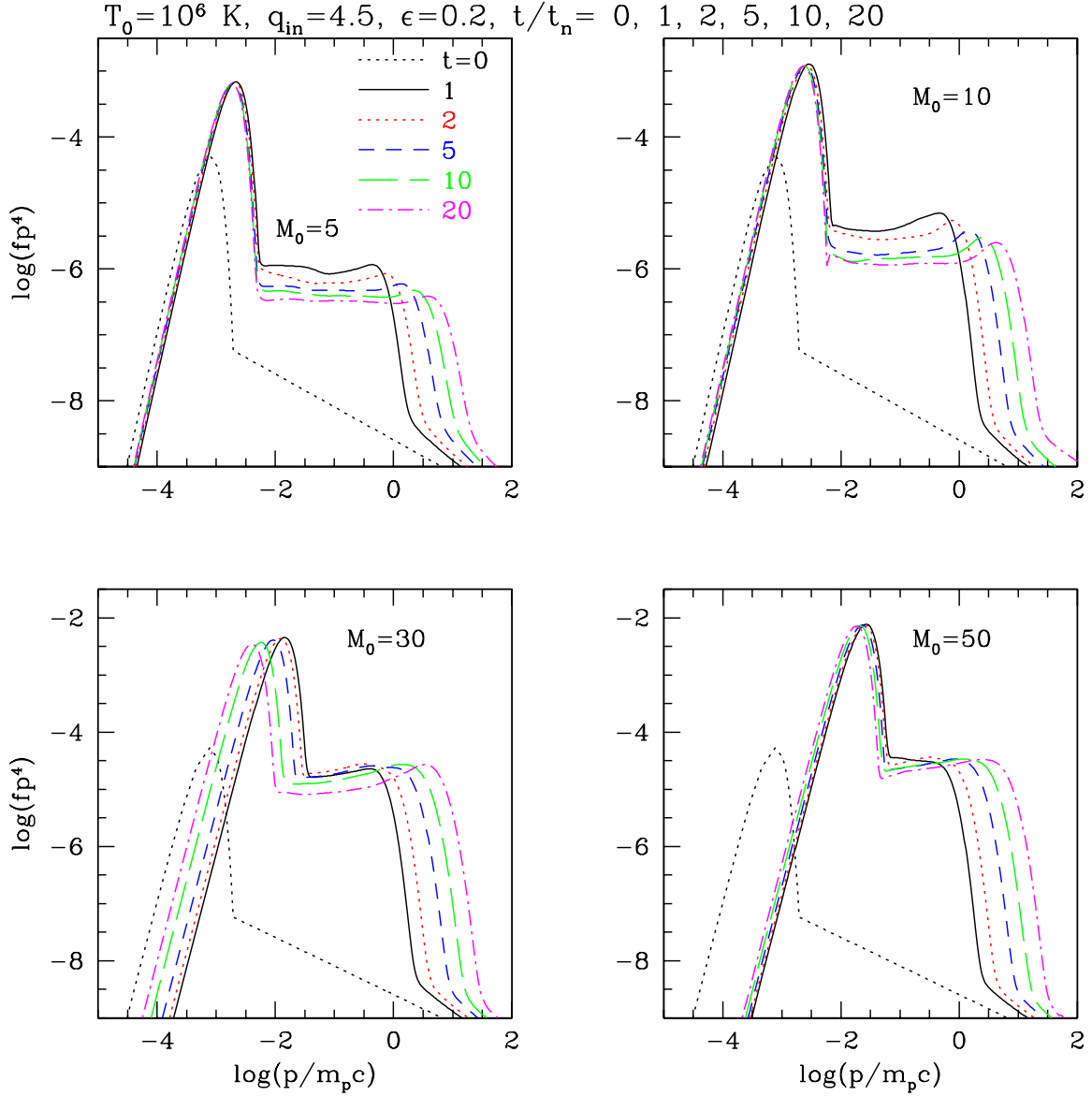


Fig. 5.— Evolution of the CR distribution function at the shock, represented as $g = p^4 f(p)$, is plotted for the models of $M_0 = 5, 10, 30,$ and 50 with $T_0 = 10^6$ K and $f_{up} \propto (p/p_M)^{-4.5}$. The CR spectrum of the preshock flow is represented by the dotted line. For all models shown here the upstream CR pressure is $P_{c,0}/P_{g,0} = 0.25$.

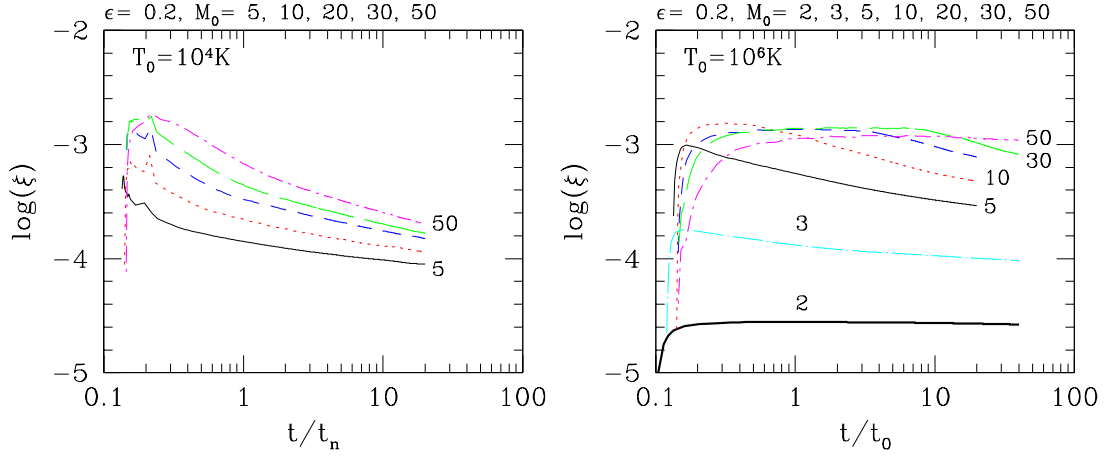


Fig. 6.— Time averaged injection efficiency, $\xi(t)$, for models without pre-existing CRs. Left panel shows the models with $M_0 = 5 - 50$ and $T_0 = 10^4$ K, while right panel shows the models with $M_0 = 2 - 50$ and $T_0 = 10^6$ K.

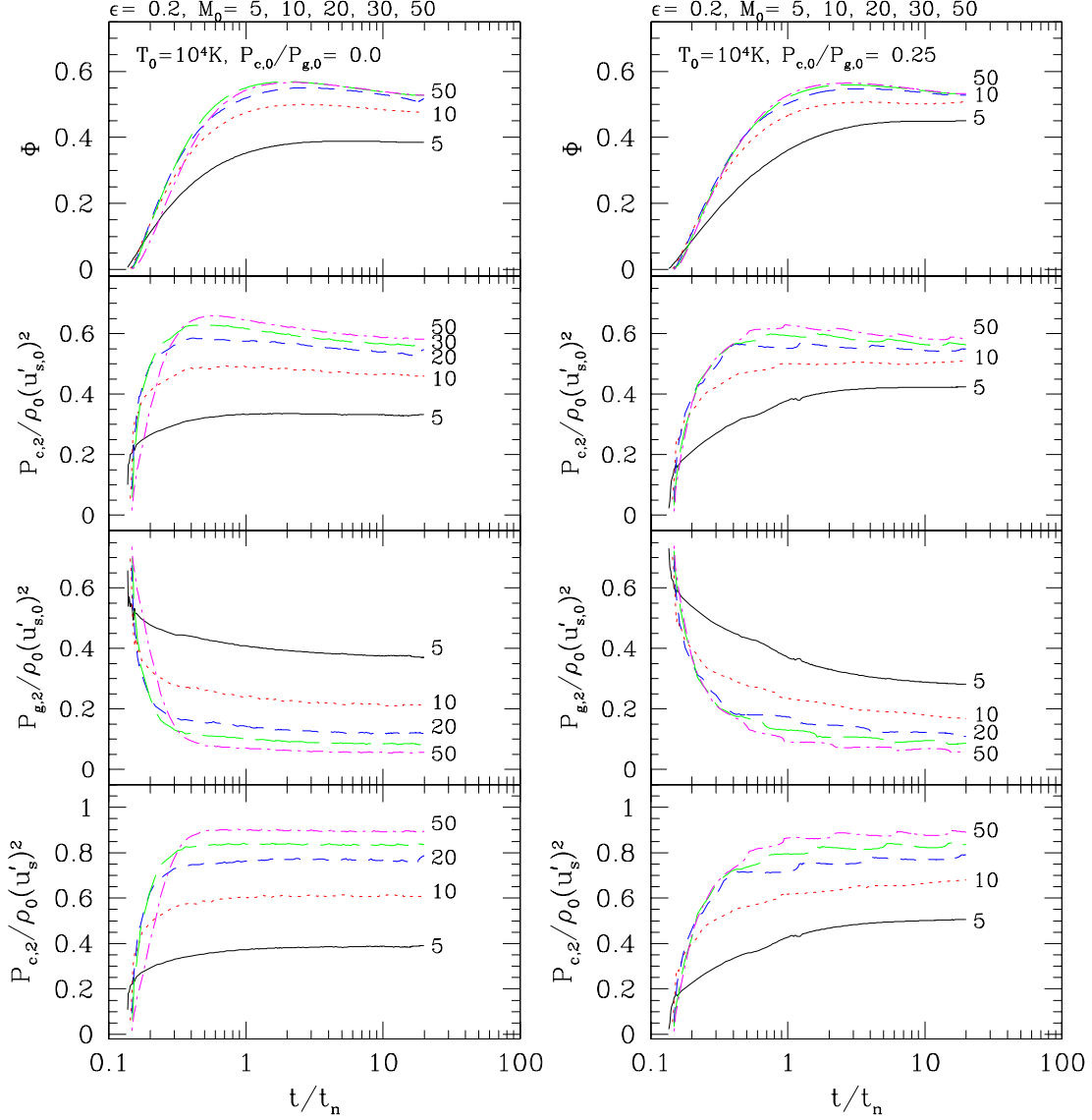


Fig. 7.— The ratio of total CR energy in the simulation box to the kinetic energy in the initial shock rest frame that has entered the simulation box from upstream, $\Phi(t)$, the postshock CR pressure, $P_{c,2}$, and gas pressure, $P_{g,2}$, in units of upstream ram pressure in the *initial* shock frame, $\rho_0 u'_{s,0}{}^2$ and the postshock CR pressure in units of upstream ram pressure in the *instantaneous* shock frame, $\rho_0 u'_s{}^2$. Left panels show the models with $M_0 = 5 - 50$ and $T_0 = 10^4$ K but without pre-existing CRs. Right panels for the same models but with the upstream CR pressure of $P_{c,0} = 0.25P_{g,0}$ and $f_{up} \propto (p/p_M)^{-4.7}$.

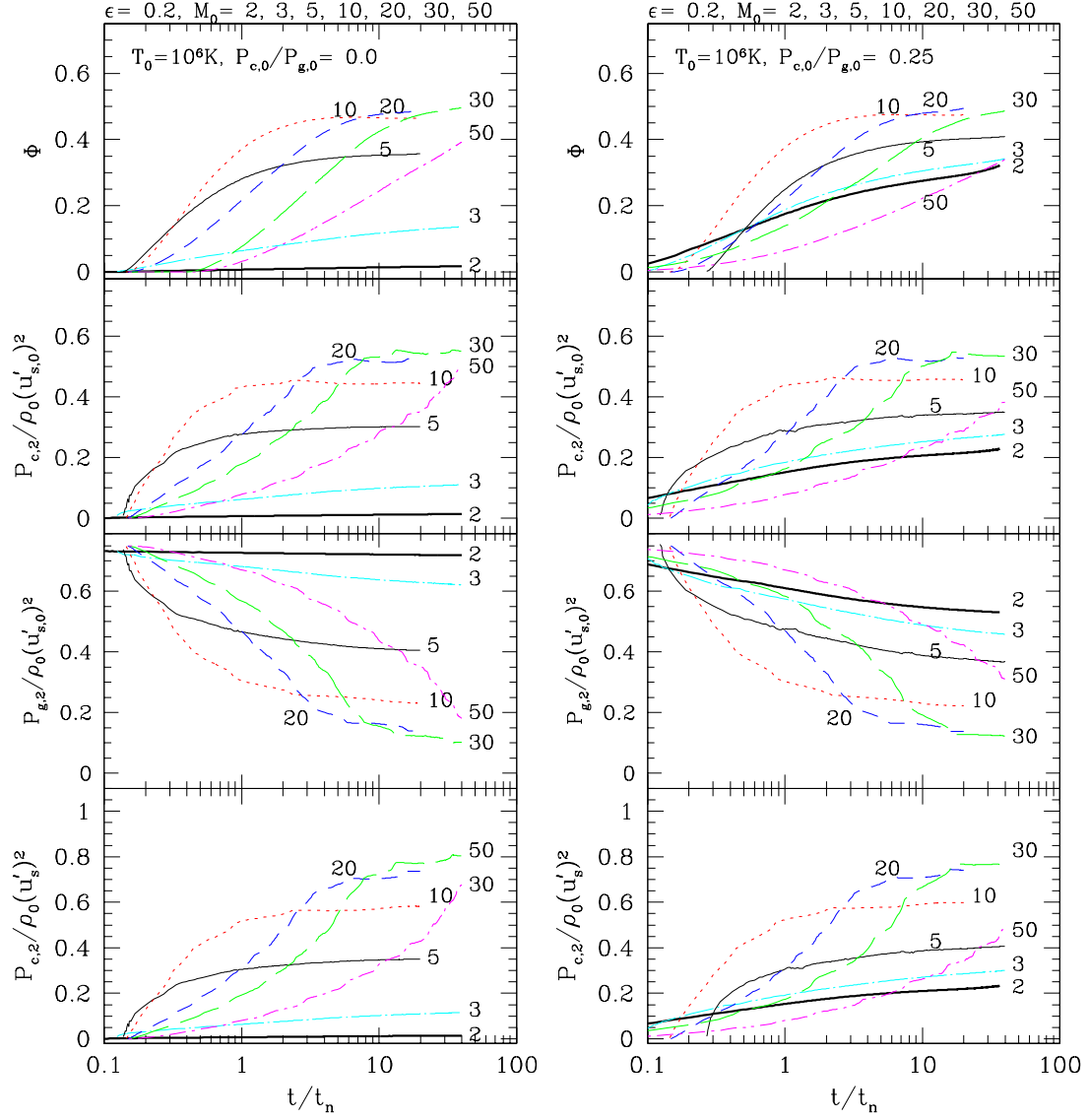


Fig. 8.— Same as figure 9 except that the models with $T_0 = 10^6$ K are shown. Left panels for the models without pre-existing CRs, while right panels for the models with $P_{c,0} = 0.25P_{g,0}$ and $f_{up} \propto (p/p_M)^{-4.5}$.

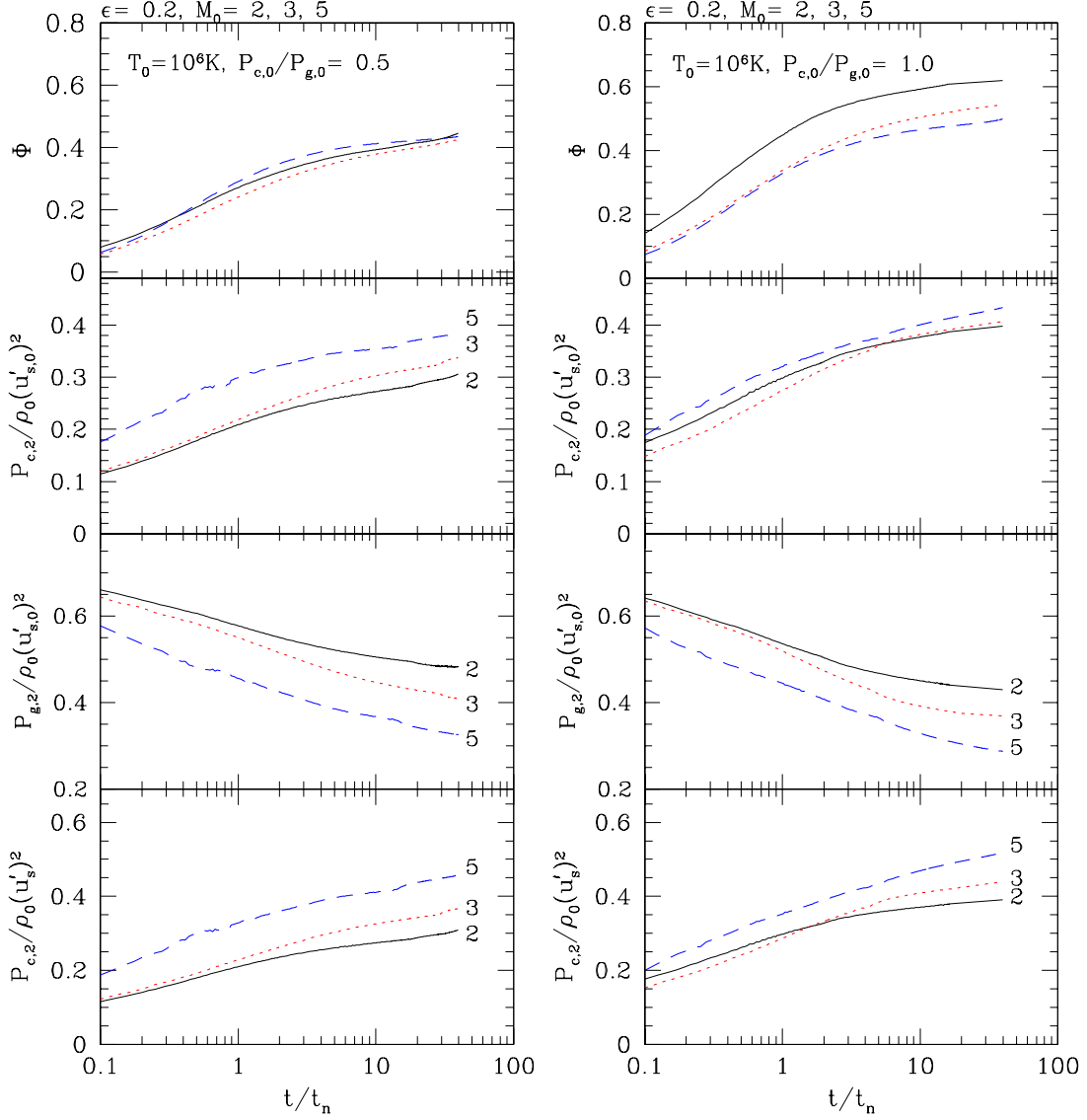


Fig. 9.— Same as figure 9 except that the low Mach models with $T_0 = 10^6$ K are shown. Left panels show the models with pre-existing CRs of $P_{c,0} = 0.5P_{g,0}$ and $f_{up} \propto (p/p_M)^{-4.4}$, while right panels for the models with $P_{c,0} = P_{g,0}$ and $f_{up} \propto (p/p_M)^{-4.3}$. Solid line is for $M_0 = 2$ model, dotted line for $M_0 = 3$ model, and dashed line for $M_0 = 5$ models.

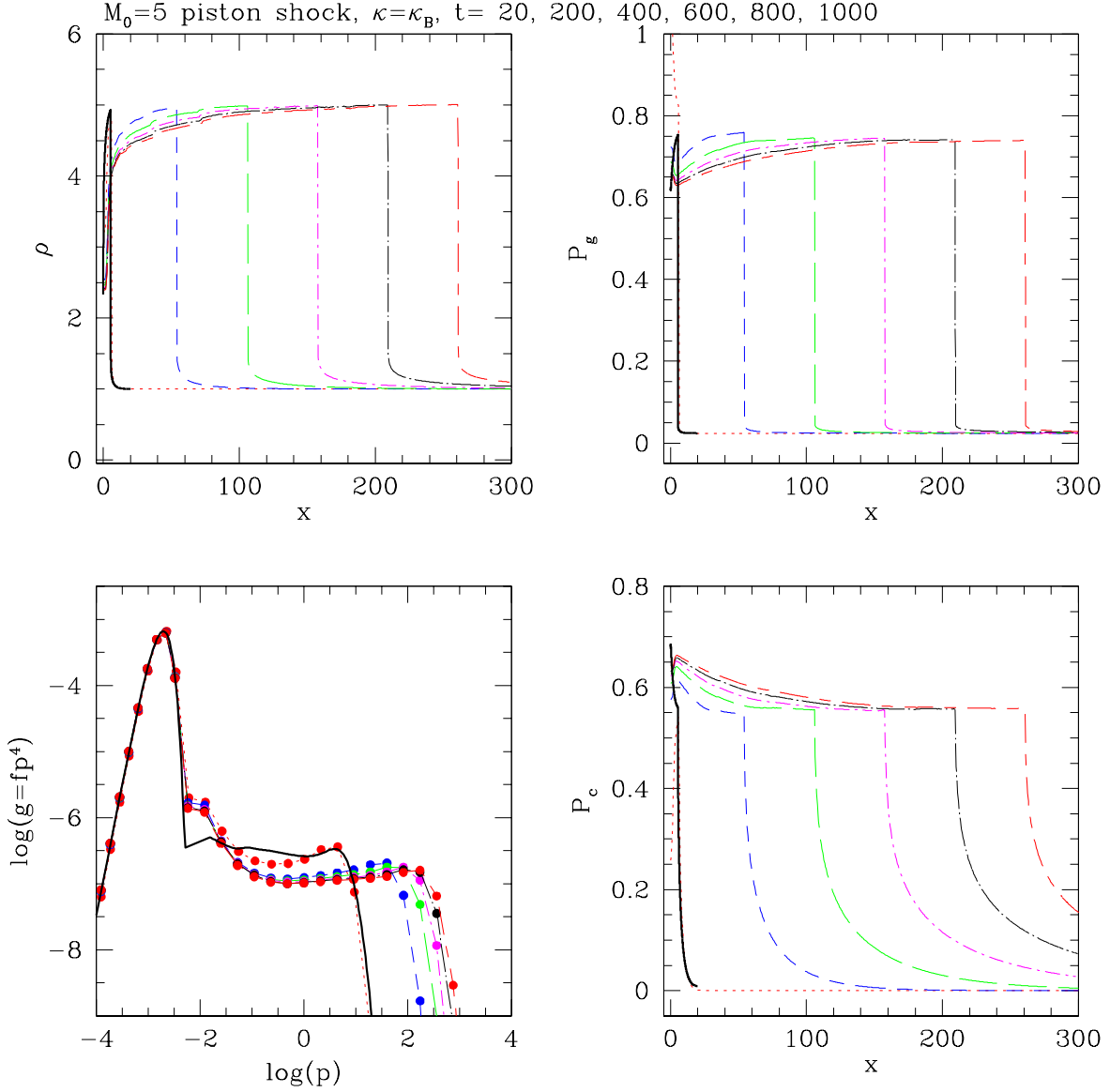


Fig. 10.— Time evolution of the $M_0 = 5$ model without pre-existing CRs calculated with "Coarse-Grained Momentum Volume" method is shown up to $t/t_n = 1000$. The leftmost profile corresponds to the earliest time, $t/t_n = 20$. For comparison, the results of "Fine-Grained Momentum Volume" simulation are shown at the same time by the heavy solid line.

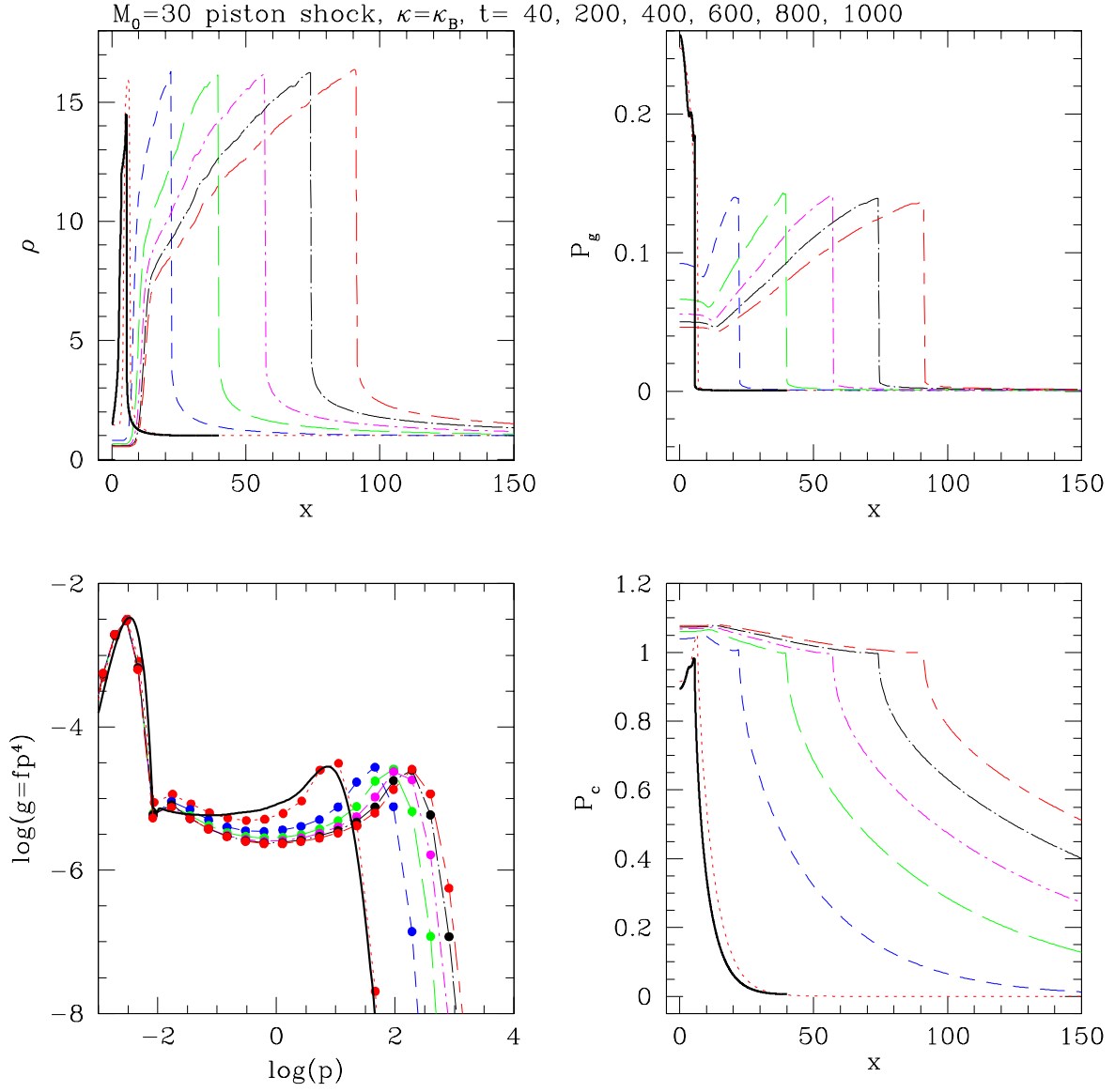


Fig. 11.— Same as Figure 10 except $M_0 = 30$. The results from two simulations are compared at $t/t_n = 40$.

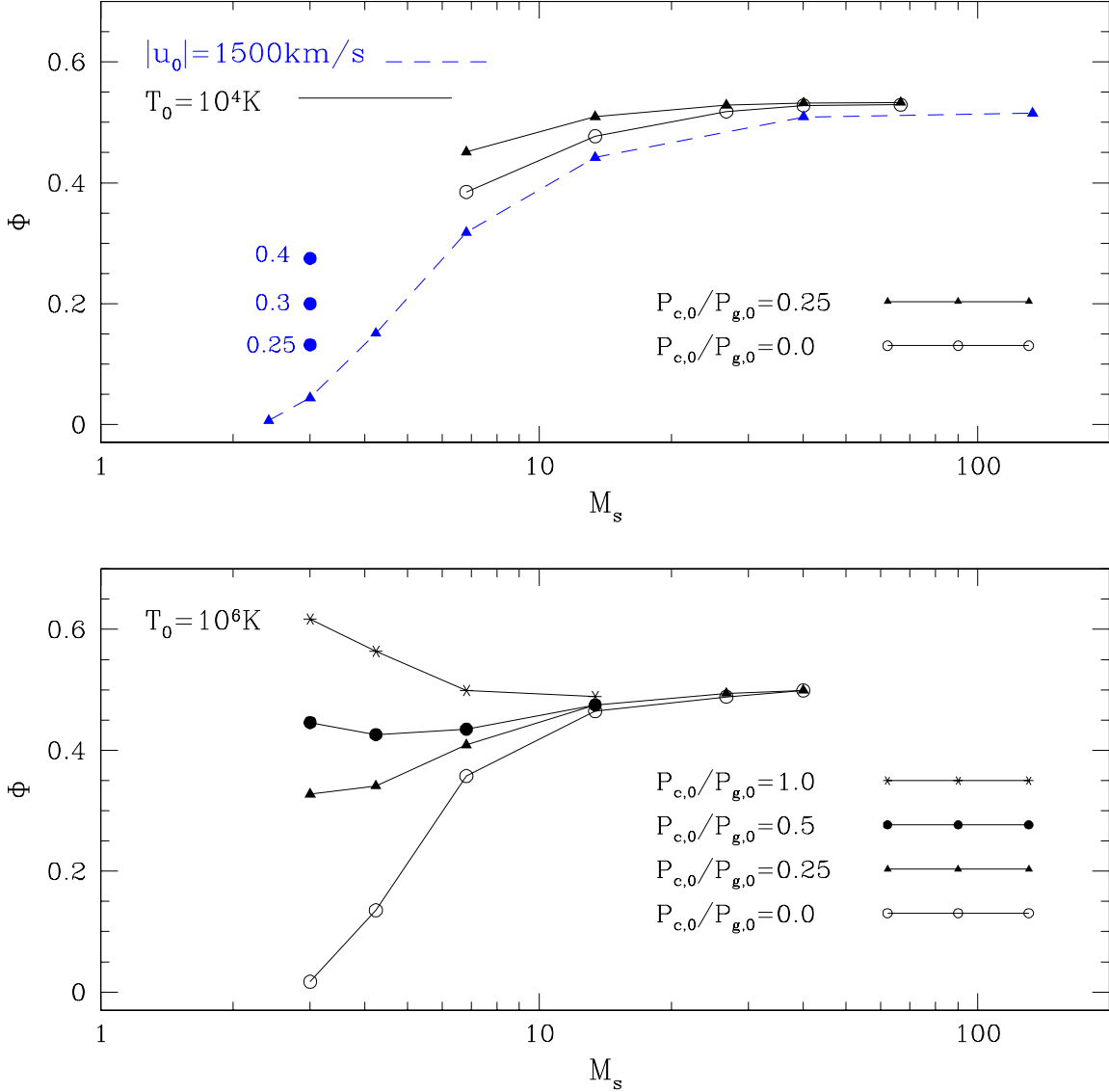


Fig. 12.— The CR energy ratio, Φ , at the simulation termination time of our simulations as a function of the shock Mach number, M_s . *Upper panel:* models with $T_0 = 10^4 \text{ K}$, $u_s = (15 \text{ km s}^{-1})M_s$, $\epsilon = 0.2$, and no pre-existing CRs (solid line with open circles), models with $T_0 = 10^4 \text{ K}$, $u_s = (15 \text{ km s}^{-1})M_s$, $\epsilon = 0.2$, and $P_{c,0} = 0.25P_{g,0}$ (solid line with filled triangles). For comparison we also show “constant u_0 models with $|u_0| = 1500 \text{ km s}^{-1}$, $T_0 = 10^4 \text{ K}(100/M_0)$, $\epsilon = 0.2$, and no pre-existing CRs in the upper panel (dashed line with filled triangles). Three filled circles are labeled with the value of $\epsilon = 0.25, 0.3, 0.4$ and for the models with $M_s = 3$, $T_0 = 5 \times 10^5 \text{ K}$ and no pre-existing CRs. *Lower panel:* models with $T_0 = 10^6 \text{ K}$, $u_s = (150 \text{ km s}^{-1})M_s$, $\epsilon = 0.2$, and a various level of pre-existing CR pressure. See Table 1 for the relation between the accretion Mach number M_0 and M_s .

Table 1. Model Parameters for Flows Upstream of Shocks

T_0 (K)	$ u_0 $ (km s ⁻¹)	M_0^a	M_s^b	$P_{c,0}/P_{g,0}$	q_{in}^c
10^4	$(15)M_0$	5, 10, 20, 30, 50	6.8, 13.4, 26.7, 40., 66.7	0.0	...
10^4	$(15)M_0$	5, 10, 20, 30, 50	6.8, 13.4, 26.7, 40., 66.7	0.25	4.7
10^6	$(150)M_0$	2, 3, 5, 10, 20, 30, 50	3., 4.2, 6.8, 13.4, 26.7, 40., 66.7	0.0	...
10^6	$(150)M_0$	2, 3, 5, 10, 20, 30, 50	3., 4.2, 6.8, 13.4, 26.7, 40., 66.7	0.25	4.5
10^6	$(150)M_0$	2, 3, 5, 10	3., 4.2, 6.8, 13.4	0.5	4.4
10^6	$(150)M_0$	2, 3, 5, 10	3., 4.2, 6.8, 13.4	1.0	4.3
$10^8 M_0^{-2}$	1500	1.5, 2, 3, 5, 10, 30, 100	2.4, 3., 4.2, 6.8, 13.4, 40., 133.	0.0	...

^aMach number of piston with respect to inflow.

^bMach number of initial gas shock with respect to infall.

^cPower-law index of upstream CR population, *i.e.*, $f_{up} \propto p^{-q_{in}}$.